A FINITE ELEMENT MESH OPTIMIZATION PROCEDURE USING A THERMAL EXPANSION ANALOGY

by

Vinh Dinh Nguyen

Thesis submitted to the Faculty of the

Virginia Polytechnic Institute and State University

in partial fulfillment of the requirements for the degree of

Master of Science

in

Mechanical Engineering

APPROVED:

Charles E. Knight, Chairman

Reginald G. Mitchiner

Hamilton H. Mabie

August, 1985

Blacksburg, Virginia

A FINITE ELEMENT MESH OPTIMIZATION PROCEDURE USING A THERMAL EXPANSION ANALOGY

by

Vinh Dinh Nguyen

Charles E. Knight, Chairman

Mechanical Engineering

(ABSTRACT)

Finite element optimum meshes are synthesized by the use of thermal expansion principles in conjunction with an analogous temperature field computed from the element strain energy contents. Elements having high strain energy contents are shrunk and those with low strain energy contents are expanded until all elements contain the same amount of strain energy. Deviatoric strain energy is also used in place of the strain energy as the objective function for the optimization method. Both objective functions yield significant improvements of the meshes after only a few iterations. In one test case, the errors in the maximum stresses are reduced by more than 1/3 after 1 iteration. In another test case, the error in the stress concentration factor is reduced by more than 3/4 after 7 iterations.

ACKNOWLEGEMENTS

The author wishes to dedicate this work to his parents, brothers, and sister for their never ending love, support, and encouragement.

The author also wishes to thank Dr. Charles E. Knight for his valuable advice, patience, and guidance, without which this paper would not be possible. The author also wishes to extend his gratitude to Dr. Reginald G. Mitchiner and Dr. Hamilton H. Mabie for serving on his advisory committee.

Finally, the author is indebted to Mitchel Keil, Ashit Gandhi, and Robert Williams for their superb help with the figures in this thesis.

TABLE OF CONTENTS

LIST OF FIGURES

LIST OF TABLES

1. INTRODUCTION

Since the finite element method involves the discretization of a continuum into a finite number of finite sized elements, the accuracy of the solution depends a great deal on the sizes and distribution of the elements used. A coarse mesh with a few large elements may yield results totally inaccurate, thus rendering the analysis completely useless. On the other hand, any specified accuracy can be achieved within practical limits with a mesh of a large enough number of uniformly, arbitrarily small elements. However, solving such a large problem may require too much computation time and computer disk space, especially the latter. Frequently, the size of a model is limited by the computer storage available to the user. Therefore, the user may have to use a relatively coarse mesh and yet must produce accurate solutions. Thus, the main question is how to achieve maximum accuracy with a given number of elements. The solution to this dilemma is mesh optimization.

The basis of mesh optimization is to use elements of various sizes to model the continuum in such a way that the best accuracy is achieved for a given number of elements. Since the early 1970's, researchers have sought and found many different ways to arrive at optimum meshes. Some included the nodal coordinates as unknowns in the potential energy equation and tried to minimize the overall potential energy of the mesh. Others used iterative schemes to minimize certain objective functions or to reduce the estimated errors to below a specified level. While they can be used to arrive at optimum meshes, most of these methods are difficult to implement and to use; some are downright impractical.

This paper will present yet another method of mesh optimization which is easy to implement and easy to use. The proposed method is based on the premise that a sufficient condition for a optimum mesh is that all elements in the mesh contain the same amount of some energy function. The method uses an iterative scheme based on a thermal expansion analogy to level the energy contents in all elements by shrinking elements in areas of high energy densities and expanding elements in areas of low energy densities. Strain energy and deviatoric strain energy will be investigated as possible energy functions for the method.

The next chapter features a review of methods of mesh optimization published by previous researchers. The basic principles of the methods, as well as their strengths and weaknesses will be discussed. A detailed explanation of the proposed method, along with a brief review of the finite element formulation is presented in Chapter 3. Chapter 4 describes the implementation of the proposed method on program MESS at Virginia Polytechnic Institute and State University. The chapter starts with a brief description of the original program, followed by a more detailed description of the modified version. In Chapter 5, two case studies with different levels of stress concentration are considered in order to determine some parameters of the optimization method and to verify the optimality of the optimized mesh. A brief study on modeling of problems with concentrated loads is also included at the end of the chapter.

2. LITERATURE REVIEW

After the birth of the finite element method in the 1950's, the first 20 years or so were devoted to establishing the foundation of the method and to expanding the applicability of the method to most engineering fields. It was not until the early 1970's that researchers started to try to improve the accuracy of the finite element method through mesh optimization.

Shephard [1] defined mesh optimization as an algorithmic procedure for the generation of a finite element discretization that yields the required accuracy for the minimum amount of effort. Shephard's paper is a review of the history of mesh optimization dating from the early inclusive criteria methods to the present day's domination of criterion based iterative schemes. The principles of these two classes of methods will be illustrated in this chapter through a few examples of each class.

The very first attempts at mesh optimization were done through mathematical formulations in the inclusive criteria methods. Early researchers tried to arrive at the optimum mesh through mathematical manipulations of the potential energy functional [2]:

$$\Pi_p = \sum_{e=1}^{EL} \left[\frac{1}{2} \{d\}_e^T \left(\int_{V_e} [B]^T [E][B] dV \right) \{d\}_e \right] - \{R\}^T \{d\} \qquad (2.1)$$

where EL is the total number of elements,

V_e is the volume of element e,

$\{d\}_e$ is the displacement vector for element e,

[B] is the element strain-node displacement matrix,

[E] is the matrix of material stiffness,

{R} is the external load vector, and

{d} is the global displacement vector.

According to the principle of minimum potential energy, the solution to the finite element problem is some admissible displacement field d which makes Π_p a minimum; the lower the minimum is, the closer the finite element solution is to the theoretical solution. Since the finite element solution varies depending on the discretization and thus each discretization may result in a different minimum for Π_p, the best solution is that discretization which yields the lowest possible minimum for Π_p. McNeice and Marcal [2] proposed to include the nodal coordinates, as well as the nodal displacements as variables in the energy functional. Minimization of Π_p requires that:

$$\delta\Pi_p = 0 \tag{2.2}$$

Since Π_p is a function of both the nodal displacements and the nodal coordinates, equation 2.2 translates into:

$$\frac{\partial\Pi_p}{\partial d_i} = 0 \qquad , i=1,2,\ldots,n \tag{2.3}$$

$$\frac{\partial\Pi_p}{\partial x_j} = 0 \qquad , j=1,2,\ldots,m \tag{2.4}$$

where n is the total number of unrestrained nodal displacements and m the total number of unconstrained nodal coordinates. Equation 2.3 yields the usual relationship:

$$[K]\{d\} - \{R\} = 0 \tag{2.5}$$

where [K] is the global stiffness matrix,

{d} is the global displacement matrix, and

{R} is the external load vector.

Meanwhile, equation 2.4 results in a less familiar set of equations:

$$\frac{1}{2}\{d\}^T \frac{\partial[K]^T}{\partial x_j}\{d\} - \frac{\partial\{R\}^T}{\partial x_j}\{d\} = 0 \quad , j=1,2,\ldots,m \tag{2.6}$$

The optimal solution should satisfy both equations 2.5 and 2.6. While the first set of equations is linear and very easy to solve, the second set of equations is highly nonlinear, compounded by the nonlinearity of the boundary constraints to preserve the domain geometry. Except for very simple problems, it is extremely difficult to find a solution to equation 2.6 by an explicit method. As a result, many researchers have resorted to numerical procedures to solve the equation. Carroll and Barker [3] used an iterative scheme involving a gradient search technique to minimize the residual of equation 2.6. Turcke and McNeice [4] used another iterative scheme with a direct search technique. While these numerical techniques can be used to produce the solution to equations 2.5 and 2.6, they are not, according to Shephard, very reliable for problems with se-

vere nonlinearities. Furthermore, even with all possible efficiency built-in, these methods still prove to be so lengthy and expensive for the general case that they cannot be considered practical.

Deterred by the difficulties in solving equation 2.6, recent researchers turned to criterion based iterative schemes. In this approach, the problem is first modeled with a coarse starting mesh. Additional degrees of freedom are subsequently introduced to the mesh in such a way as to satisfy some optimization criteria. These iterative methods differ from one another mainly in the optimization criteria selected and the method of mesh enrichment chosen. Based upon mesh enrichment, the iterative methods can be divided into two groups: selective refinement methods and contour methods. The first group, as suggested by the name, starts with a coarse mesh and then refines it in certain areas, usually to bring some objective function down below a prespecified level. The elements in areas where the objective function is above the limit are subdivided and then further subdivided in each iteration until the objective function falls below the limit everywhere in the mesh. Babuska and Rheinboldt [5] and Babuska [6] investigated an L shaped domain subjected to Dirichlet boundary conditions. The authors defined the pointwise error due to discretization as:

$$\varepsilon = d - d^* \tag{2.7}$$

where ε is the discretization error,

d is the theoretical solution, and

d^* is the finite element solution.

Since d is the theoretical solution, $\nabla^2(d) = 0$ and therefore,

$$-K = \nabla^2\varepsilon \tag{2.8}$$

where K is a Dirac function. The solution to equation (2.8) is a sum of two functions:

$$\varepsilon = \eta + \phi \tag{2.9}$$

where η is a well known harmonic function representing the error due to linear interpolation, and ϕ is the discretization error. Using the concept of a cell, which contains the area tributary to a single node, the authors used difference equations to arrive at an expression for the upper bound of the unknown function ϕ. This upper bound, along with the known harmonic function η, constitutes the approximate error for the cell. Elements in cells of high errors are subdivided and the iteration is repeated until all errors fall below the prespecified level. Carey and Humphrey [7] considered force related residuals on the elemental level as the objective function to be minimized. The authors defined the residuals as sum of two components: residuals inside the elements and residuals on the interelement boundaries. The first component is defined as:

$$R_{V_e} = k_1 \int_{V_e} (D(d^*) - f)^2 dV_e \tag{2.10}$$

where V_e is the element volume,

d^* is the finite element solution,

$D(\ )$ denotes the operation of the differential equation,

f is the external load, and

k_1 is some unspecified constant.

The second component is defined as:

$$R_{\Gamma_e} = k_2 \int_{\Gamma_e} (T_e - T_n)^2 d\Gamma_e \tag{2.11}$$

where Γ_e is the element boundary,

T_e are the tractions inside element e,

T_n are the tractions from neighboring elements, and

k_2 is some unspecified constant.

Again, new degrees of freedom are introduced into areas of high residuals by subdividing the elements in these areas. Depending on the mesh refinement scheme involved, the elements can have only fixed shapes and discreet levels of element sizes. These mathematical constraints on the elements can, and often do, result in a mesh not as optimal as theoretically possible for the number of elements used.

The second group of iterative methods is characterized by the use of the contours of certain solution parameters from the previous analysis as the guide for mesh generation in the following iteration. Turcke and McNeice [8] investigated the optimum meshes of one and two dimensional problems as obtained through the solution of equations 2.5 and 2.6. The

authors found that the optimum meshes have elements aligned approximately along the contours of the strain energy density and that all elements in an optimum mesh should have the same total strain energy. Shephard, Gallagher, and Abel [9] incorporated interactive computer graphics into the contour method to facilitate mesh generation. They used an automatic mesh generator to generate the new mesh based on the strain energy contours of the previous analysis. Jara-Almonte [10] also studied the contour method, using the contours of strain energy density, deviatoric strain energy density, and the Von Mises equivalent stress, with the total element contents of these objective functions serving as parameters for the optimization criterion. He defined the optimum mesh as that in which all elements contain the same amount of one of the objective functions. Jara-Almonte concluded that while all three objective functions can be used to produce the optimum meshes, the strain energy density and the deviatoric strain energy density contours yield approximately the same results, and both yield more accurate results than do the contours of the Von Mises equivalent stress. The contour methods, while not as mathematically involved, are superior to the previously discussed methods in that the new mesh can be totally independent from the previous mesh. As a result, greater improvements can be made in each iteration. One drawback of the contour methods, however, is the time and the difficulty in defining the mesh for each iteration. The methods require either complicated and time consuming mesh generation routines in the case of automatic mesh generation or extensive input from the user in the case of mesh generation using interactive graphics. Furthermore, the element sizes and shapes must conform to some criteria such as the contour

spacings and the number of nodes on each contour line. Consequently, the optimum meshes obtained through the contour methods, like those from the selective refinement methods, may not be the best mesh possible with the given number of elements.

Like the contour methods proposed by Jara-Almonte, the iterative method proposed in this paper uses the element strain energy contents or the element deviatoric strain energy contents as possible parameters of the optimization criteria. Unlike other iterative methods, however, the proposed method does not introduce any additional degrees of freedom to the mesh, but instead tries to make the most efficient use of a given number of elements by arriving at the optimum mesh through a thermal strain analogy. As a result, no mesh refinement schemes are needed and the elements are free to change in size and shape while maintaining continuity until the optimum mesh is obtained. From the discussion above, it is evident that the proposed method, other than serving as an optimization method by itself, can also be incorporated into other optimization schemes to further improve the accuracy of the solution.

3. THEORY

The optimum mesh is defined as one in which all elements have nearly equal strain energy contents or deviatoric strain energy contents, depending on the energy function selected. To simplify terminologies, both the strain energy density and the deviatoric strain energy density henceforth will be referred to as the general energy density indicator (GEDI) in the discussions applicable to both energy functions. Similarly, both the strain energy content and the deviatoric strain energy content in an element will be referred to as the general energy content indicator (GECI).

The optimization method uses an iterative scheme based on analysis results from the actual problem to arrive at the optimum mesh by use of a thermal expansion analogy. Each iteration involves the solutions of two problems, the actual problem and the expansion problem. First, the actual problem, with boundary conditions and loads, is solved. The element GECIs computed for the actual problem are then used to calculate an initial strain load vector. The expansion problem uses this load vector, along with additional boundary constraints imposed to preserve the overall domain geometry to shrink or expand element volumes and level the GECI distribution. The displacements from this analogous thermal expansion problem are then used to update the mesh for the actual problem in the next iteration. The procedure is repeated until some convergence criterion is met. This chapter will explain in detail the formulation and the solution of both the actual problem and the expansion problem, followed by a selection of the convergence criterion.

3.1. Actual Problem

The only element considered in the paper is an isoparametric, plane stress, four node quadrilateral 2-D element. However, it seems reasonable that the method can be extended to other 1-D or 2-D elements as well. A brief review of the formulation of the element as used in MESS [10] is presented in this section, followed by the solution procedure of the finite element problem. Interested readers can refer to Cook [11] and Zienkiewicz [12] for a more detailed explanation. The calculations of solution parameters such as Cauchy stresses, deviatoric stresses, strain energy, and deviatoric strain energy are also outlined.

3.1.1. Isoparametric Formulation

The isoparametric element is formulated in an intrinsic coordinate space ξ-η as a square element centered at the origin of the coordinate system. Figure 3-1 shows an element in the ξ-η space. When mapped into the global coordinate system in the x-y space, the element in Fig. 3-1 transforms to that in Fig. 3-2. In the x-y space, axes ξ and η are no longer orthogonal and the element may assume any arbitrary quadrilateral shape. The x-y coordinates of points inside the element comprise a position field which can be thought of as a vector surface function over the square domain in the ξ-η space. From the known x-y coordinates of the corner nodes, the x-y coordinates of any other point inside the element (in the ξ-η space) can be calculated using an interpolation matrix:

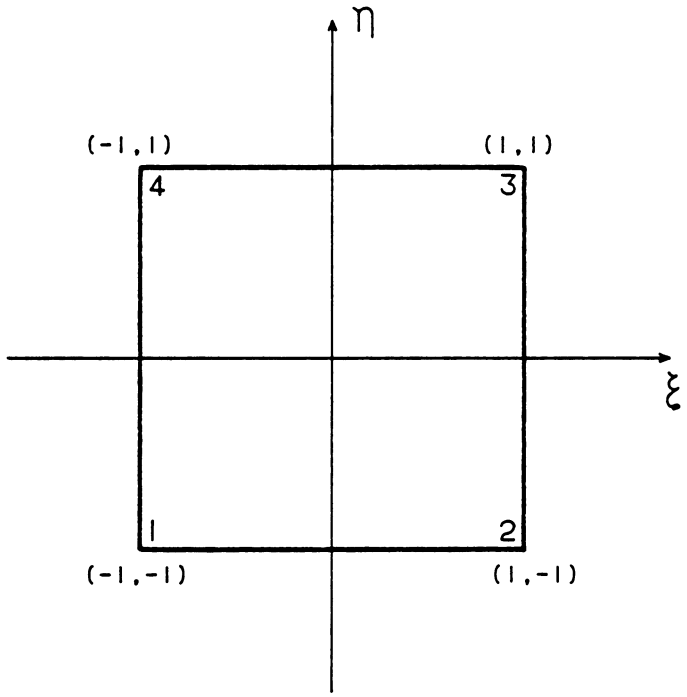

Figure 3-1. An Isoparametric Element in the Intrinsic Coordinate Space

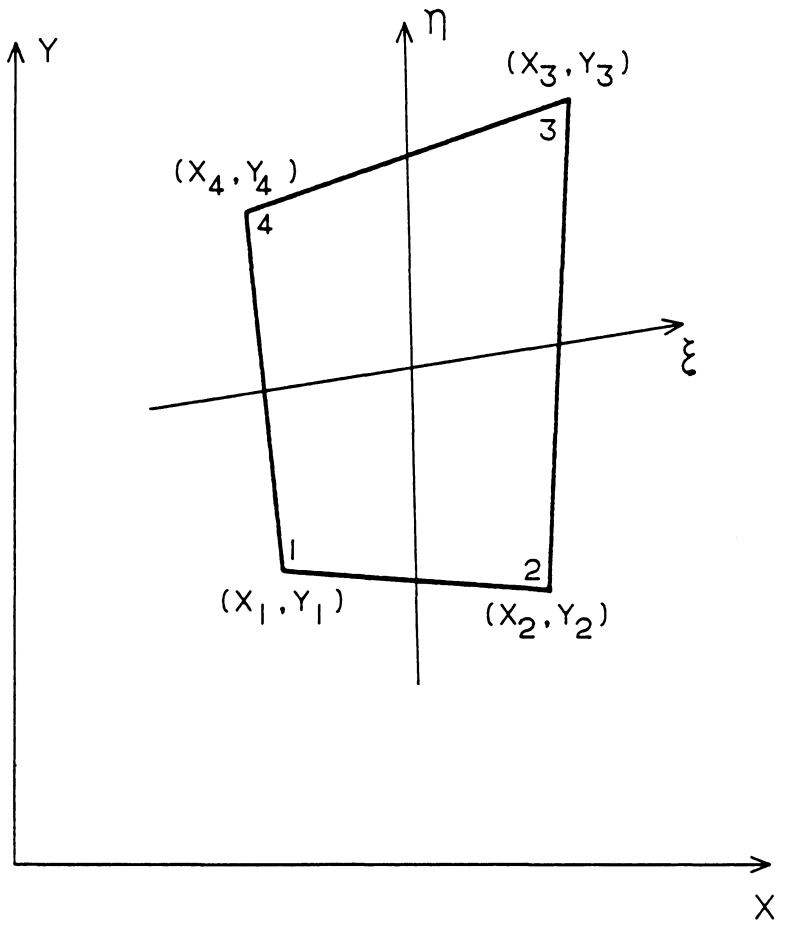

Figure 3-2. An Isoparametric Element in the Global Coordinate Space

$$\begin{Bmatrix} x \\ y \end{Bmatrix} = [N]\{c\} \tag{3.1}$$

where {c} is a vector containing the x-y coordinates of the corner nodes:

$$\{c\}^T = \{x_1\ y_1\ x_2\ y_2\ x_3\ y_3\ x_4\ y_4\}^T \tag{3.2}$$

Matrix [N] is the interpolation matrix:

$$[N] = \begin{bmatrix} N_1 & 0 & N_2 & 0 & N_3 & 0 & N_4 & 0 \\ 0 & N_1 & 0 & N_2 & 0 & N_3 & 0 & N_4 \end{bmatrix} \tag{3.3}$$

where N_1, N_2, N_3, and N_4 are shape functions derived from the Lagrange interpolation formula. These shape functions are functions of the ξ-η coordinates of an arbitrary point inside the element:

$$N_1 = \frac{1}{4}(1-\xi)(1-\eta) \tag{3.4 a}$$

$$N_2 = \frac{1}{4}(1+\xi)(1-\eta) \tag{3.4 b}$$

$$N_3 = \frac{1}{4}(1+\xi)(1+\eta) \tag{3.4 c}$$

$$N_4 = \frac{1}{4}(1-\xi)(1+\eta) \tag{3.4 d}$$

Using the same interpolation matrix, the displacement field is calculated as follows:

$$\begin{Bmatrix} u \\ v \end{Bmatrix} = [N]\{d\} \tag{3.5}$$

where {d} is the vector containing the displacement components of the corner nodes:

$$\{d\}^T = \{u_1\ v_1\ u_2\ v_2\ u_3\ v_3\ u_4\ v_4\}^T \tag{3.6}$$

Matrix [N] is the same as that used in the position field formula; hence arises the term isoparametric.

The calculation of stress and strain requires the differentiation of equation 3.5 with respect to x and y. However, since only the ξ-η coordinates are treated as variables in the isoparametric formulation, equation 3.5 can only be differentiated with respect to ξ and η:

$$\begin{Bmatrix} u_{,\xi} \\ u_{,\eta} \\ v_{,\xi} \\ v_{,\eta} \end{Bmatrix} = \begin{bmatrix} N_{1,\xi} & 0 & N_{2,\xi} & 0 & N_{3,\xi} & 0 & N_{4,\xi} & 0 \\ N_{1,\eta} & 0 & N_{2,\eta} & 0 & N_{3,\eta} & 0 & N_{4,\eta} & 0 \\ 0 & N_{1,\xi} & 0 & N_{2,\xi} & 0 & N_{3,\xi} & 0 & N_{4,\xi} \\ 0 & N_{1,\eta} & 0 & N_{2,\eta} & 0 & N_{3,\eta} & 0 & N_{4,\eta} \end{bmatrix} \begin{Bmatrix} u_1 \\ v_1 \\ u_2 \\ v_2 \\ u_3 \\ v_3 \\ u_4 \\ v_4 \end{Bmatrix} \tag{3.7}$$

where the subscripts ,ξ and ,η denote the partial differentiation with respect to ξ and η, respectively. Therefore, the partial derivatives with respect to x and y must be obtained in an indirect manner from those in ξ and η.

Let ω be an arbitrary function of x and y, the chain rule yields the following equations:

$$\frac{\partial \omega}{\partial \xi} = \frac{\partial \omega}{\partial x}\frac{\partial x}{\partial \xi} + \frac{\partial \omega}{\partial y}\frac{\partial y}{\partial \xi} \tag{3.8 a}$$

$$\frac{\partial \omega}{\partial \eta} = \frac{\partial \omega}{\partial x}\frac{\partial x}{\partial \eta} + \frac{\partial \omega}{\partial y}\frac{\partial y}{\partial \eta} \tag{3.8 b}$$

Written in matrix form, equations 3.9 become:

$$\begin{Bmatrix} \omega_{,\xi} \\ \omega_{,\eta} \end{Bmatrix} = [J] \begin{Bmatrix} \omega_{,x} \\ \omega_{,y} \end{Bmatrix} \tag{3.9}$$

Thus, equation 3.9 transforms the partial derivatives in the two coordinate spaces. The transform matrix [J] is called the Jacobian matrix:

$$[J] = \begin{bmatrix} x_{,\xi} & y_{,\xi} \\ x_{,\eta} & y_{,\eta} \end{bmatrix} = \begin{bmatrix} J_{11} & J_{12} \\ J_{21} & J_{22} \end{bmatrix} \tag{3.10}$$

Written in terms of the shape functions and nodal coordinates, the Jacobian matrix becomes:

$$[J] = \begin{bmatrix} N_{1,\xi} & N_{2,\xi} & N_{3,\xi} & N_{4,\xi} \\ N_{1,\eta} & N_{2,\eta} & N_{3,\eta} & N_{4,\eta} \end{bmatrix} \begin{bmatrix} X_1 & Y_1 \\ X_2 & Y_2 \\ X_3 & Y_3 \\ X_4 & Y_4 \end{bmatrix} \tag{3.11}$$

The Jacobian matrix is non-singular, and thus has an inverse:

$$[\Gamma] = [J]^{-1} = \begin{bmatrix} \Gamma_{11} & \Gamma_{12} \\ \Gamma_{21} & \Gamma_{22} \end{bmatrix} \tag{3.12}$$

Therefore, the partial derivatives of the displacement field in the x-y space can be written in terms of those in the ξ-η space:

$$\begin{Bmatrix} u_{,x} \\ u_{,y} \\ v_{,x} \\ v_{,y} \end{Bmatrix} = \begin{bmatrix} \Gamma_{11} & \Gamma_{12} & 0 & 0 \\ \Gamma_{21} & \Gamma_{22} & 0 & 0 \\ 0 & 0 & \Gamma_{11} & \Gamma_{12} \\ 0 & 0 & \Gamma_{21} & \Gamma_{22} \end{bmatrix} \begin{Bmatrix} u_{,\xi} \\ u_{,\eta} \\ v_{,\xi} \\ v_{,\eta} \end{Bmatrix} \tag{3.13}$$

The equations for strains written in matrix form is:

$$\{\varepsilon\} = \begin{bmatrix} 1 & 0 & 0 & 0 \\ 0 & 0 & 0 & 1 \\ 0 & 1 & 1 & 0 \end{bmatrix} \begin{Bmatrix} u_{,x} \\ u_{,y} \\ v_{,x} \\ v_{,y} \end{Bmatrix} \tag{3.14}$$

where $\{\varepsilon\}^T = \{\varepsilon_x \ \varepsilon_y \ \gamma_{xy}\}^T$

Applying equations 3.7 and 3.13 to equation 3.14, the strain can also be written as:

$$\{\varepsilon\} = [B]\ \{d\} \tag{3.15}$$

where {d} is the nodal displacement vector for the element. Matrix [B] is called the strain-node displacement matrix and is the product of the matrices in equations 3.14, 3.13, and 3.7, in that order. It relates the strains at any point inside the element to the displacement components of the corner nodes.

The stiffness matrix of the element can now be computed using the following equation based upon minimization of potential energy [11]:

$$[k] = \int_{-1}^{1}\int_{-1}^{1} [B]^T[E][B]tJd\xi d\eta \tag{3.16}$$

where t is the thickness of the element, assumed to be unity by MESS. J is the determinant of the Jacobian matrix:

$$J = J_{11}J_{22} - J_{21}J_{12} \tag{3.17}$$

Matrix [E] is the matrix of material stiffness. For a plane stress element with isotropic material properties:

$$[E] = \frac{E}{(1-\nu^2)} \begin{bmatrix} 1 & \nu & 0 \\ \nu & 1 & 0 \\ 0 & 0 & \frac{(1-\nu)}{2} \end{bmatrix} \tag{3.18}$$

Where E is the Young's modulus and ν is the Poisson's ratio. After the elemental stiffness matrices are assembled into a global stiffness matrix representing the structure, the nodal displacements can be calculated [11]:

$$\{D\} = [K]^{-1}\{R\} \tag{3.19}$$

where $\{D\}$ is the global node displacement vector,

$[K]^{-1}$ is the inverse of the global stiffness matrix, and

$\{R\}$ is the external nodal load vector.

3.1.2. Calculation of Solution Parameters

The optimization method requires the computation of the element GECI to formulate the expansion problem. First, the stresses from the actual problem have to be calculated. Combining equation 3.15 with the constitutive equation $\{\sigma\} = [E]\{\varepsilon\}$, the formula of the Cauchy stresses becomes:

$$\{\sigma\} = [E][B]\{d\} \tag{3.20}$$

The stresses at any point inside the element can be computed by using the ξ-η coordinates of that point in the shape functions. MESS computes the stresses at the Gauss points, which are labeled as points I, II, III, and IV in Fig. 3-3. The stresses at other points are obtained by fitting a smoothing surface through the Gauss point values. The interested reader

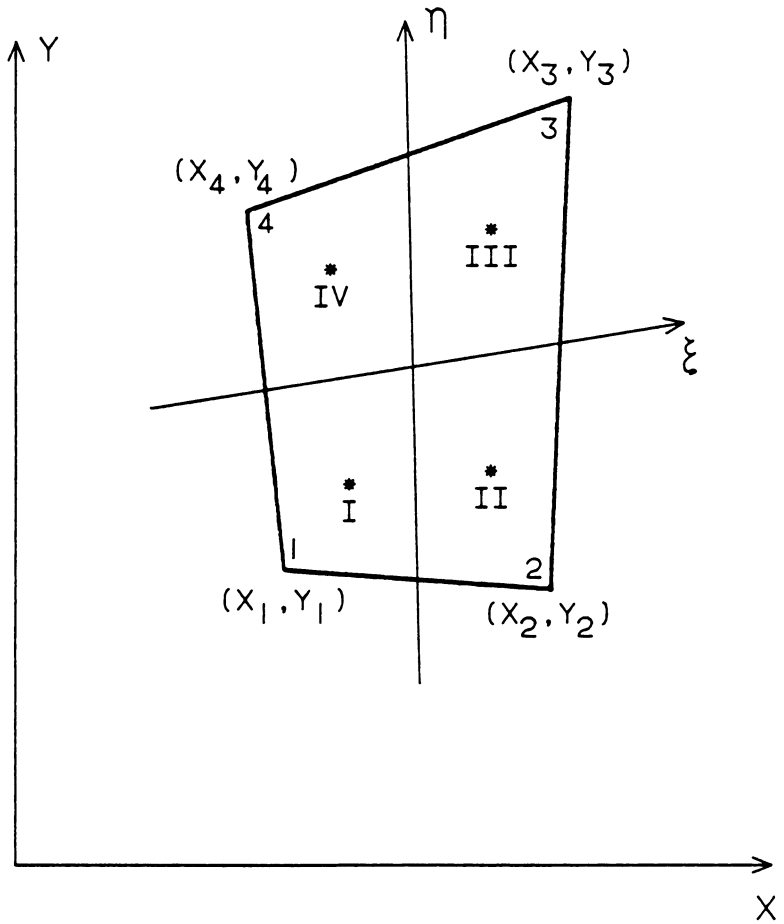

Figure 3-3. Locations of Gauss Points in an Element

is referred to Hinton and Campbell [13] for a discussion of the smoothing surface. The stresses at the element centroid, however, are not obtained from the smoothing surface. Instead, they can be obtained more accurately by averaging the Gauss point stresses.

The deviatoric stresses are the Cauchy stresses with the hydrostatic stress subtracted. The deviatoric stresses at any point can be calculated from the Cauchy stresses. For 2-D plane stress cases, the deviatoric stresses are calculated as follows:

$$\sigma'_x = \sigma_x - \frac{1}{3}(\sigma_x + \sigma_y) \qquad (3.21\ a)$$

$$\sigma'_y = \sigma_y - \frac{1}{3}(\sigma_x + \sigma_y) \qquad (3.21\ b)$$

$$\sigma'_z = -\frac{1}{3}(\sigma_x + \sigma_y) \qquad (3.21\ c)$$

$$\tau'_{xy} = \tau_{xy} \qquad (3.21\ d)$$

where σ_x, σ_y, and τ_{xy} are the Cauchy stresses, and prime ($'$) indicates deviatoric components.

The strain energy density, which is a scalar function, can be calculated using the following equation [11]:

$$U = \frac{1}{2}\{\varepsilon\}^T[E]\{\varepsilon\} \qquad (3.22)$$

For computational purposes, it is desirable to rewrite the strain energy density as a function of the Cauchy stresses since these quantities are already calculated by MESS. The following equations are two alternative forms of the constitutive equation:

$$\{\sigma\} = [E]\{\varepsilon\} \tag{3.23 a}$$

$$\{\varepsilon\}^T = \{\sigma\}^T[C]^T \tag{3.23 b}$$

where [C] is the matrix of material compliances. For the plane stress element with isotropic material properties:

$$[C] = \frac{1}{E}\begin{bmatrix} 1 & -\nu & 0 \\ -\nu & 1 & 0 \\ 0 & 0 & 2(1+\nu) \end{bmatrix} \tag{3.24}$$

Combining equations 3.23 and 3.24, and making use of the symmetry of [C], the strain energy density can be written as:

$$U = \frac{1}{2}\{\sigma\}^T[C]\{\sigma\} \tag{3.25}$$

The deviatoric strain energy density can be calculated in the same fashion, with the deviatoric stresses substituted for the Cauchy stresses.

MESS computes the GEDI at the Gauss points since the stresses here are most accurate. Then, the GEDI at the element centroid is calculated as an average of the Gauss point values:

$$GEDI_c = \frac{1}{4}\sum_{i=1}^{4} GEDI_i \tag{3.26}$$

where $GEDI_i$ is the GEDI at individual Gauss points in an element and $GEDI_c$ is the GEDI at the element centroid. This GEDI at the element centroid

is assumed to be the average value for the element. Then, the element GECI can be calculated as follows:

$$GECI = (GEDI_c)\times(V) \tag{3.27}$$

where V is the volume of the element:

$$V = \frac{t}{2}[(X_1Y_2 + X_2Y_3 + X_3Y_4 + X_4Y_1) - (Y_1X_2 + Y_2X_3 + Y_3X_4 + Y_4X_1)] \tag{3.28}$$

where t is the thickness of the element.

3.2. Expansion Problem

The purpose of the expansion problem is to shrink elements with a high GECI and expand elements with a low GECI until the GECIs are uniform over all elements. The problem is based on the concept that the element GECIs can be converted into analogous temperatures, which can then be used to adjust the sizes of the elements as in the thermal expansion problem. The expansion problem requires the computation of two parameters: an analogous temperature for each element and an analogous coefficient of thermal expansion.

The element temperature T_e is taken to be the negative of the deviation of the GECI of the element from the average value for the entire structure:

$$T_e = -(GECI_e - GECI_{ave}) \tag{3.29}$$

According to equation 3.29, elements with a GECI higher than the average value will have a negative temperature and thus will shrink. The higher the element GECI is, the more negative the temperature becomes, and the element shrinks more. Likewise, elements with a GECI lower than the average value will have a positive temperature and will expand.

Suppose the element is free to shrink or expand, then the initial thermal strains caused by the analogous temperature are:

$$\{\varepsilon_T\} = \begin{Bmatrix} \varepsilon_{Tx} \\ \varepsilon_{Ty} \\ \gamma_{Txy} \end{Bmatrix} = \alpha \begin{Bmatrix} T_e \\ T_e \\ 0 \end{Bmatrix} \tag{3.30}$$

where α is the analogous coefficient of thermal expansion.

The selection of α is of paramount importance in the usefulness of the method. The coefficient of expansion must be established such that it is applicable to most engineering problems. Obviously, a method that requires the user to find an appropriate value of α for each new problem is not very appealing.

The selection of α is governed by two potential computational difficulties. First, due to the definition of the analogous temperature, the range of this temperature may vary greatly from problem to problem, depending on the level of energy content in the problem. When the same problem has the loading magnitude increased, the energy content, and consequently the thermal strains will increase, causing the elements to

shrink or expand more than in the case of smaller loads. This, in effect calls for a different numerical value of α for each loading magnitude in order to obtain the same relative amount of element shrinkage or expansion. Second, the problem geometry can generate stress concentrations that result in local areas of very high stresses creating very high analogous temperatures. While it is desirable that elements in area of stress concentration have high analogous temperatures so that they can shrink or expand by a great amount in each iteration, in problems with very high stress concentrations these temperatures can get so high that values of α applicable for problems with no stress concentrations can result in excessive initial strains.

From the discussion above, it is evident that the coefficient of thermal expansion must be normalized such as to eliminate the effects of load magnitudes and to reduce the geometry effects. One appropriate form of α which satisfies the requirements just stated is:

$$\alpha = \frac{\beta}{GECI_{max}} \tag{3.31}$$

where β, henceforth referred to as the expansion constant, is to be determined and $GECI_{max}$ is the GECI of the element with the maximum energy content. Applying equations 3.29 and 3.31 to equation 3.30, the thermal strains (both x and y directions) of each element becomes:

$$\varepsilon_{Tx} = \varepsilon_{Ty} = - \frac{\beta}{GECI_{max}} (GECI_e - GECI_{ave})$$

$$= -\beta \left(\frac{GECI_e}{GECI_{max}} - \frac{GECI_{ave}}{GECI_{max}} \right) \tag{3.32}$$

where $GECI_e$ is the GECI of the element under consideration and $GECI_{ave}$ is the average GECI over all elements. The two ratios in equation 3.32 are functions of problem geometry only since both the numerators and denominators change proportionally as the loading magnitude is varied. Thus, the thermal strains are now independent of the loading magnitude.

The reduction of the geometry effects can be seen more clearly by considering only the element with the highest GECI since this element experiences the greatest shrinkage. For this element equation 3.32 reduces to:

$$\varepsilon_{Tx} = \varepsilon_{Ty} = -\beta \left(1 - \frac{GECI_{ave}}{GECI_{max}} \right) \tag{3.33}$$

Equation 3.33 exhibits two important properties. First, both $GECI_{max}$ and $GECI_{ave}$ increase with the stress concentration, with the first increasing due to the presence of a stress concentration and the latter due to the increase in total energy content of the mesh. However, since stress concentrations are fairly localized effects, the increase in $GECI_{max}$ is much greater than that in $GECI_{ave}$. Consequently, the ratio of $GECI_{ave}$ to $GECI_{max}$ decreases, resulting in an increase of the strain magnitude, as desired. Second, the magnitude of the compressive strain in equation 3.33 approaches β as $GECI_{max}$ gets large and approaches zero as $GECI_{max}$ tends to $GECI_{ave}$. Therefore, the normalization has effectively reduced the range of possible compressive strains from infinitely wide to a narrow range from 0 to β. Notice that controlling the compressive strains is

more important than controlling the tensile strains because excessive compression, aided by the expansion of neighboring elements may result in some interior nodes being displaced to regions outside of the geometry domain, causing an invalid formulation of the elemental stiffness matrix. Also notice that any GECI other than $GECI_{max}$ can be used in equation 3.31 and the same normalization effect is still achieved. However, when the GECIs higher than the average value are used, the convergence will be accelerated since these GECI values decrease to the average value as the mesh converges and hence result in an increase in the numerical value of α after each iteration. $GECI_{max}$ is chosen due to the fact that it is farthest away from the average value and thus will converge to the average value with the fastest rate, thereby offering the highest acceleration for the optimization process.

The value of β remains to be selected. Since β directly controls the magnitudes of the thermal strains it must be chosen small enough so that the maximum compressive strain does not exceed the possible limit of 1. On the other hand, β must be large enough to provide reasonable convergence rates for all problems. The selection of β requires the consideration of some test problems and will be presented in chapter 5.

Now that the analogous temperatures and the coefficient of expansion have been determined, they can be used to compute a set of initial strain loads for each element [11]:

$$\{r\} = \int_{-1}^{1}\int_{-1}^{1} [B]^T[E]\{\varepsilon_T\}Jtd\xi d\eta \qquad (3.34)$$

where $\{r\}$ is the element load vector,

$[B]$ is the strain-node displacement matrix,

$[E]$ is the material stiffness matrix,

ξ,η are the intrinsic coordinates (Fig. 3-1), and

$\{\varepsilon\}$ are the initial strains.

A global load vector can be assembled from the individual element load vectors $\{r\}$ by summing at each node the contributions from all surrounding elements.

The expansion problem also requires additional boundary constraints to preserve the overall problem geometry in addition to the actual boundary conditions. These constraints consist of two groups: boundary constraints and loading constraints. The boundary constraints restrict the movement of boundary nodes to one dimensional sliding along the original domain boundary, thereby confining any change in element size or shape to the interior of the domain boundary. The loading constraints totally restrain the movements of those nodes subjected to external loading so that the points of application remain stationary, thus avoiding the task of re-calculating the actual load vector for each iteration. These constraints are created for the expansion problem just to preserve the overall problem geometry.

The expansion problem, with the initial strain load vector, the set of actual boundary conditions, and additional boundary and loading constraints, can be solved in the same manner as the actual problem. It should be noted that since both the actual problem and the expansion problem share the same set of boundary conditions, instead of being as-

sembled separately, the stiffness matrix of the expansion problem can be derived from that of the former problem by deleting or combining certain rows and columns of the actual matrix based on the additional constraints, thus saving computation time. The interested reader is referred to Cook [11] for an explanation on implementing physical constraints on the stiffness matrix. The displaced geometry resulting from the solution of the expansion problem is the improved mesh and used as the mesh for the actual problem in the next iteration.

3.3. Mesh Convergence Criterion

A convergence criterion must be established to indicate when the optimum mesh has been reached and to terminate the optimization process. The selection of the convergence criterion can be made easier by considering the properties of the optimum mesh. In such a mesh, the GECIs are uniform across all elements; therefore, the mesh configuration will not change when run through the optimization procedure. As a result, the element centroids will not move from iteration to iteration. Also, since the mesh does not change, the stress field, and consequently the energy density field, does not vary from iteration to iteration. Thus, the GEDI values at the element centroids become stationary when the mesh reaches the optimum configuration; and therefore can be selected as the parameter to be monitored in the convergence criterion:

$$\frac{\|GEDI^{i+1} - GEDI^{i}\|_2}{\|GEDI^{i+1}\|_2} \leq STOL \qquad (3.35)$$

where the superscripts i and i+1 denote steps number i and i+1, respectively and $\| \ \|_2$ denotes the second or Euclidian norm. STOL is a prespecified convergence tolerance. Like the coefficient of thermal expansion, the convergence criterion is nondimensionalized to eliminate the effect of load magnitude. Care must be taken in selecting an appropriate value of STOL. STOL too large may result in a mesh far from optimum. On the other hand, STOL too small may result in wasteful iterations that do not improve the results by any significant amount.

4. IMPLEMENTATION

The optimization procedure was implemented on program MESS (Mechanical Engineering Stress Software), which was written at Virginia Polytechnic Institute and State University. MESS is a two dimensional finite element stress analysis program based on the program called STAP introduced by Bathe and Wilson [14]. However, unlike STAP which has only the 2-D truss element and virtually no pre- or post-processing capabilities, at the time of this research MESS offers a choice of three elements: 2-D truss element, isoparametric axisymmetric element, and isoparametric 2-D plane stress element and pre- and post-processing. Also, the post-processor is interfaced to program DISPLAY of the MOVIE.BYU [15] graphics package to provide fairly advanced interactive computer graphics. The post processor offers geometry and contour plots which can be called up interactively by the user.

Figure 4-1 shows the flow chart of the original program MESS as presented by Jara-Almonte [10]. The flow chart consists of three distinct parts, each performing a separate phase of the solution process. The first part reads in node, load, and element data from the input file MESS.IN. At this point all undefined nodes and elements are generated. The element connectivity data are saved on tape IELMNT for later use. Also, a load vector for each load case is calculated and stored on tape ILOAD. In this phase, the node and element data are also stored on tape MOVIET for graphic display of the geometry if the number of elements is less than 250. The limit is imposed due to dimension limits in MOVIE.

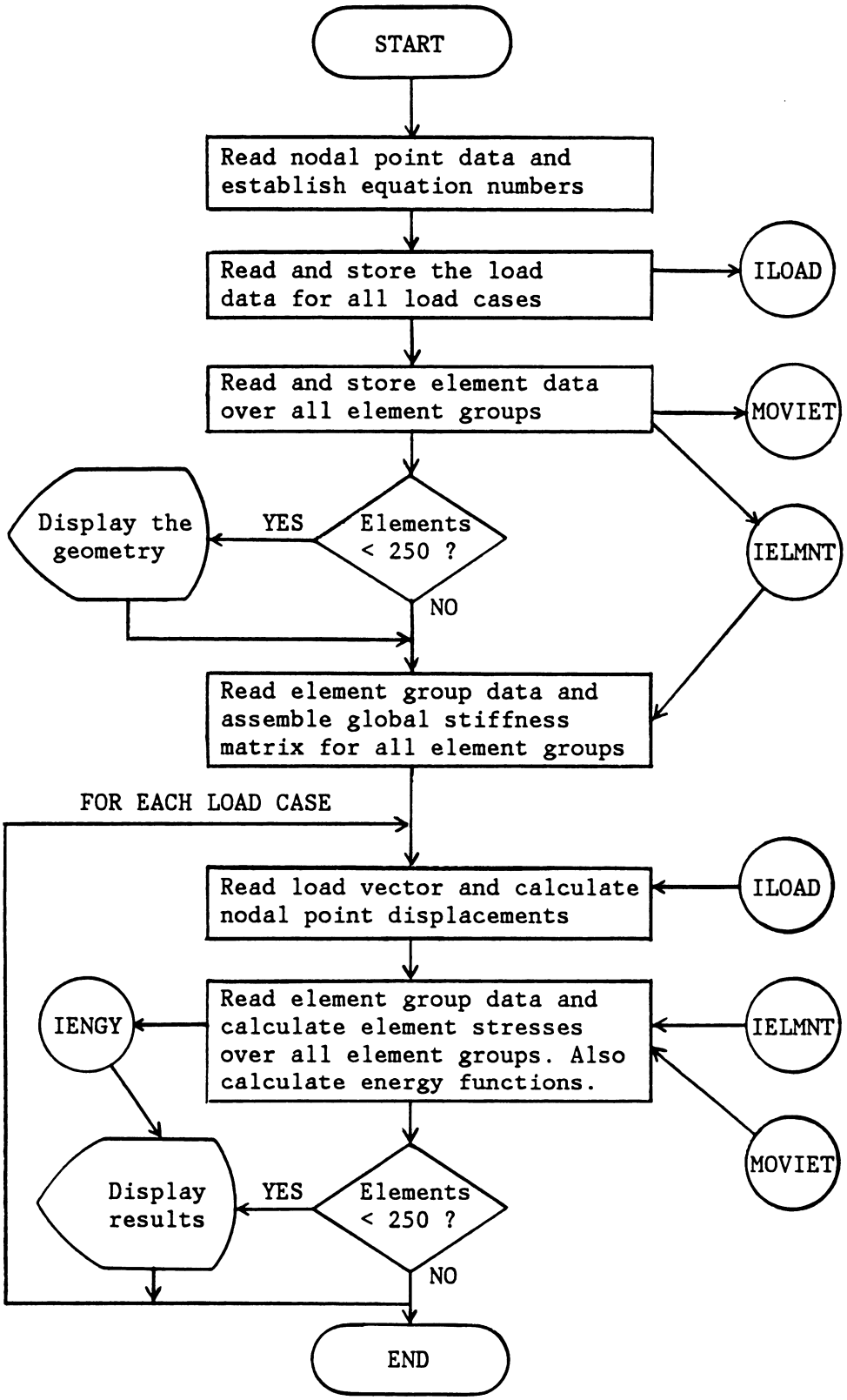

Figure 4-1. Flow Chart of Original Program MESS

The second part assembles the global stiffness matrix from the individual element stiffness matrices. First, the element connectivity data are retrieved from tape IELMNT. and the individual element stiffness matrices are calculated according to equation 3.16 in the previous chapter. Then the element matrices are integrated into a global stiffness matrix by summing, for each degree of freedom, the contribution of all elements in the mesh.

The third part solves for the nodal displacements, looping over all load cases. For each load case, the load vector is read in from tape ILOAD. Then the nodal displacements are solved using a modified Gauss elimination technique. The stress components calculated by MESS include the Cauchy stresses, the deviatoric stresses, and the Von Mises equivalent stress. The energy functions calculated are the strain energy density, the deviatoric strain energy density, the element strain energy content, and the element deviatoric strain energy content. These stresses and strain energy functions can be displayed in contour plots, along with the displaced geometry.

To implement the optimization procedure, program MESS must be expanded to accommodate the expansion problem. Figures 4-2a and 4-2b shows the flow chart of the modified program. As can be seen in the figure, the general structure of the program was left intact. Only minor changes and additions were made in each of the three parts of the program, which are described in the following paragraphs.

In addition to the boundary conditions, the first part now also reads in the additional constraints to be imposed on the expansion problem. If the geometry contains circular arcs, the arc data must also be read

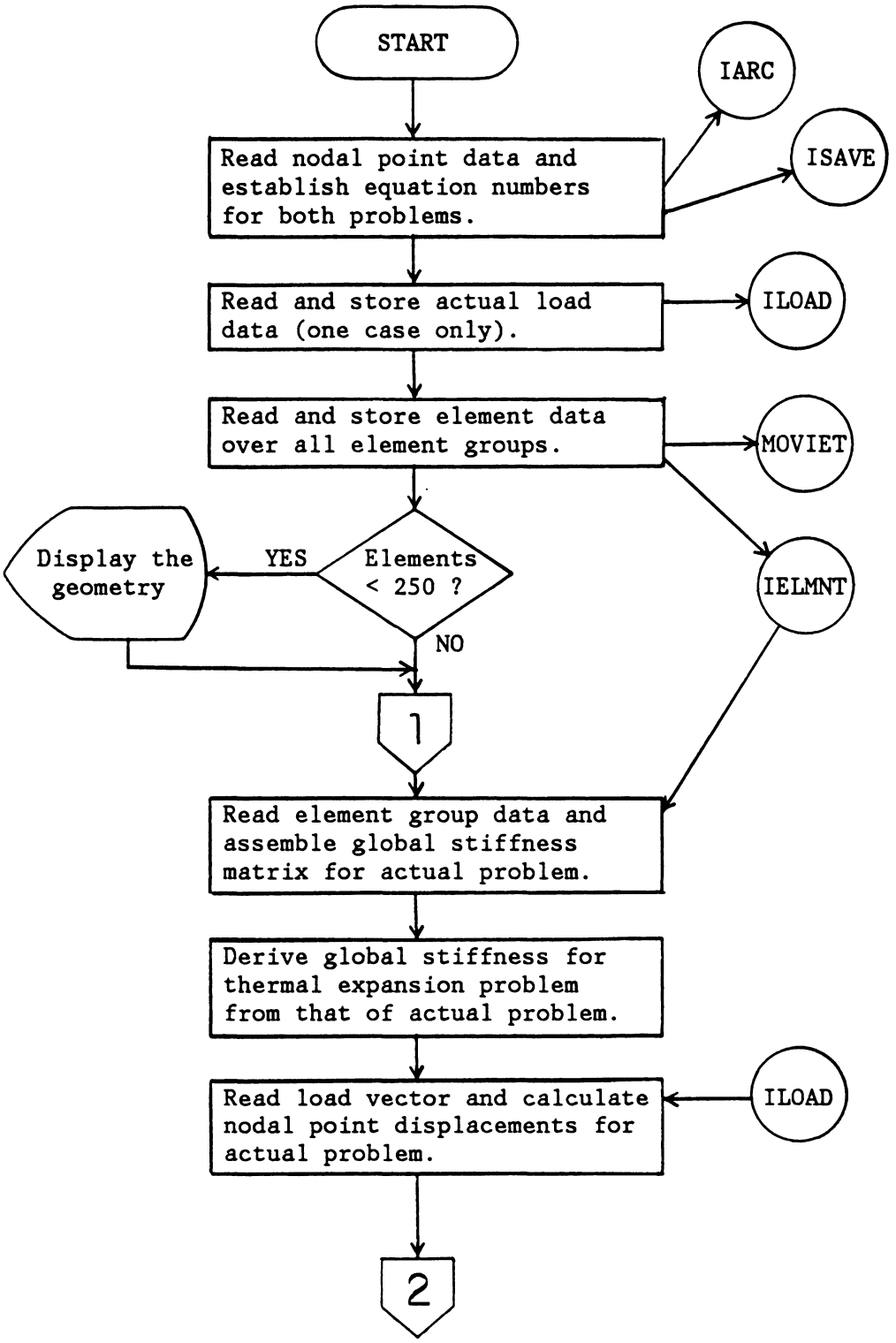

Figure 4-2a. Flow Chart of Modified Program MESS

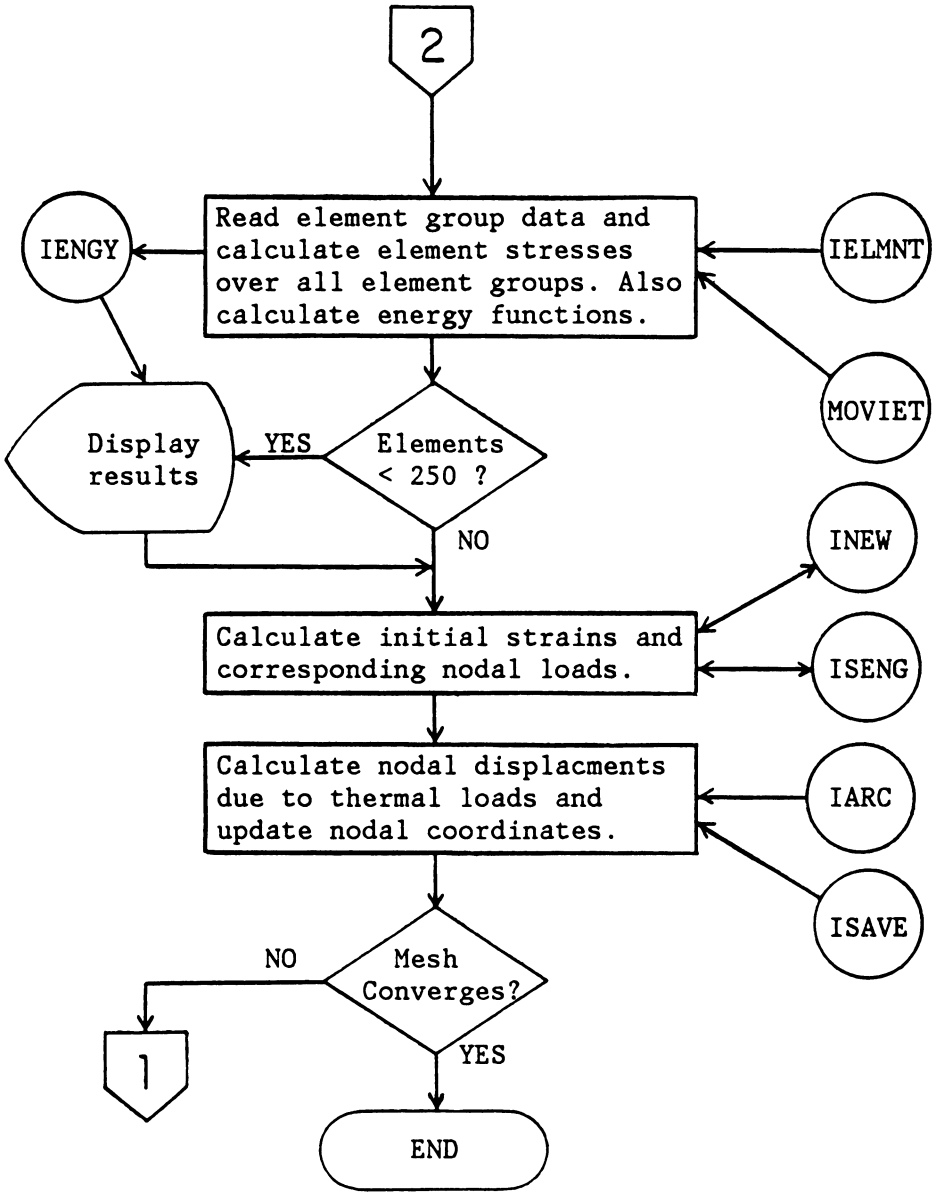

Figure 4-2b. Flow Chart of Modified Program MESS (Continued)

in. These data are needed because the nodes on the arcs may only slide along the tangent with the arcs in the expansion problem, resulting in a change in the arc radii after each iteration. To preserve geometry, the arc radii must be scaled back to the original value. Therefore, the arc data needed include the number of arcs in the problem, the nodes on the arcs, the arc radii, and the coordinates of the centers of the arcs. These data are stored in tape IARC.

The multiple load case capability is eliminated since the configuration of the optimum mesh depends on the load case, thus it may be better to start off with a fresh mesh for each load case. As a result, tapes ILOAD now contains only one load vector: the load vector of the actual problem.

The second part of the program now not only assembles the stiffness matrix for the actual problem but also derives the stiffness matrix of the expansion problem from that of the actual problem. A subroutine CONSTRUCT was written to accomplish this task by deleting or combining certain rows and columns of the actual stiffness matrix in accord with the additional constraints.

The third part now solves both problems. First, the actual problem is solved to obtain the nodal displacements, the stresses, and the energy functions. From these energy functions, the initial strain load vector is calculated as explained in the previous chapter. The stiffness matrix and load vector of the expansion problem are then passed to the Gauss elimination subroutine to solve for the nodal displacements due to thermal expansion. Subroutine MODIFY was added to the program to update the nodal coordinates after each iteration by adding the nodal displacements due

to thermal expansion to the current nodal coordinates of the actual problem. Subroutine MODIFY also scales the arc radii as previously discussed. The updated nodal coordinates are then stored on tape ISAVE, to be recalled in the next iteration.

The third part of the program also checks for convergence of the mesh. The element centroidal energy densities of the current step are stored on tape INEW while those of the previous step are stored on tape ISENG. These energy densities are used in the convergence criterion. If the mesh is converged, the program stops and prints out the most current solution to the actual problem as the optimal solution. If not the program loops back to part two and reassembles the stiffness matrices based on the updated nodal coordinates, and proceeds with the next iteration.

5. CASE STUDIES

As stated in chapter 3, the optimal procedure contains a constant to be determined, namely the expansion constant β. Since β is basically a scale factor for the element shrinkage or expansion, it directly affects the convergence rate of the mesh. A small β restricts the change in the mesh from iteration to iteration. As a result, it may take a large number of iterations to reach the optimum mesh. On the other hand, a very large β can create excessive oscillations in the mesh, leading to divergence. Therefore, it is conceivable that there is an optimal value of β for which convergence is assured and the convergence rate is fastest. Furthermore, since the coefficient of expansion α was normalized to allow for variations of strain magnitudes for different problem geometries, the convergence rate of the method may still depend on problem types. Consequently, problems with different types of stress distributions may have different optimal values for β. Therefore, a convergence study must be performed to find a range of β which provides reasonable convergence rates for most problems.

Test cases with different stress distributions will serve two purposes: first the selection of β, and second the verification of the optimality of the optimized mesh.

Two test cases with well documented theoretical solutions were selected. The first test case is a thick walled cylindrical pressure vessel as shown in Fig. 5-1. The pressure vessel has an inner radius, b, of 1 in. (25.4 mm) and an outer radius, a, of 2 in. (50.8 mm). The vessel is subjected to an internal pressure of 10.0 kpsi (68.9 MPa). Neglecting

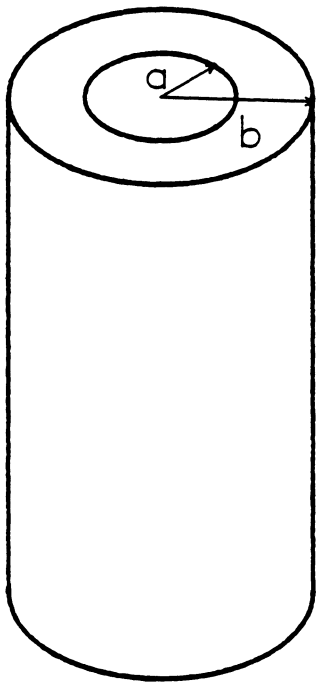

Figure 5-1. First Test Case

the end effects, a cross section of the vessel can be modeled as a 2-D problem. This test case contains no stress concentrations anywhere and therefore was selected to represent the class of problems with no stress concentrations.

The second test case is a bar with a center hole, subjected to tensile loads at two ends as shown in Fig. 5-2. The bar has dimensions of 9 in. x 6 in. x 1 in. (229 mm x 152 mm x 25.4 mm) with a center hole of 3 in. (76.2 mm) diameter. The tensile loads at the ends are distributed loads with a magnitude of 4,000 lb/in. (700,500 N/m). The center hole provides fairly high stress concentrations at the top and the bottom of the hole. This test case was chosen to represent problems with stress concentrations.

Each of these test cases were optimized using both the strain energy (SE) criterion and the deviatoric strain energy (DSE) criterion and the convergence behaviors were compared in order to arrive at a value or range of values for β applicable to most problems and for both criteria. The optimality of the optimum meshes will also be checked to verify the validity of the methods and to choose the better criterion if possible. The rest of this chapter will be devoted to the presentation of the results from the convergence studies and the verification of the validity of the optimization method.

5.1. Convergence Studies

There are two possible modes of convergence: monotonic convergence and oscillatory convergence. In an optimum mesh, each element has an

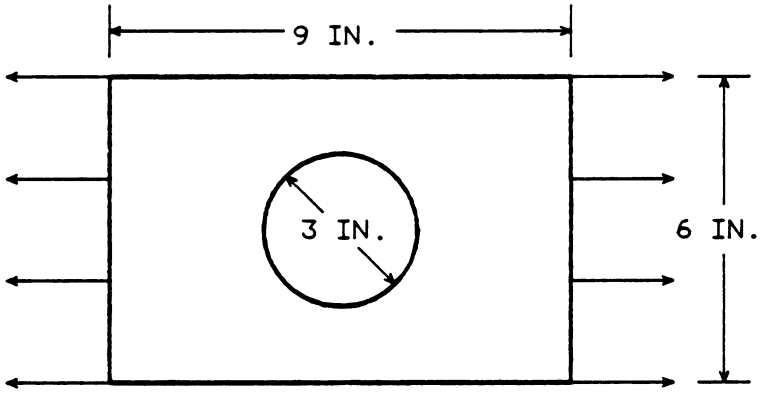

Figure 5-2. Second Test Case

"optimal" size. Monotonic convergence occurs when β is selected small enough that all elements in the mesh converge to their respective "optimal" size without overshoot in any iteration. Oscillatory convergence occurs when β is selected large enough to result in a small overshoot in some iterations, which will eventually die out. If they do not die out, the mesh diverges. Monotonic convergence is better than oscillatory convergence in that it assures convergence while oscillatory convergence may become divergent if the overshoots increase. However, it is more likely that the fastest convergence rate would occur in the oscillatory region since larger values of β result in greater shrinkage and expansion of most elements while creating only small oscillations of some elements. The overall effect can be a faster convergence rate.

Two convergence studies are performed for each test case, one study for the SE criterion and the other for the DSE criterion. In each convergence study, β is varied from 0.5 to 2.0 in steps of 0.1. For each β, the test case is optimized and the number of iterations required to reach the optimum mesh is recorded.

5.1.1. First Test Case

A cross section of the pressure vessel may be modeled as a 2-D problem. Utilizing the geometrical symmetry of the problem, only a quarter of the cross section needs to be modeled, provided that appropriate boundary conditions are applied to preserve symmetry of the cross section. A relatively coarse and uniform mesh is used to model the upper right quarter of the cross section. This starting mesh is shown in Fig.

5-3. Only 20 elements are used, 4 across the wall thickness and 5 along the arcs. The elements are assumed to have the following material properties:

Young's Modulus = 30×10^6 psi (207 GPa)

Poisson's Ratio = 0.3

In the actual problem of this test case, nodes on the axes of symmetry are confined to sliding along their respective axes of symmetry. These boundary conditions are imposed on the mesh to preserve the symmetry of the cross section. In the expansion problem, the nodes on the inner arc, being subjected to external loads, theoretically must be constrained in all directions. However, due to the circular symmetry of the problem, these nodes can only slide radially but not along the arc and thus need to be constrained in the radial direction only.

First, the SE criterion is used to optimize the test case. The results of this convergence study are plotted in Fig. 5-4 for different values of the convergence tolerance STOL. The vertical axis is the number of iterations required for convergence and the horizontal axis is the expansion constant β. Note that although the results can only be discrete points since one can have only whole numbers of iterations, a smooth curve is faired through the data points in Fig. 5-4 for ease of comparison. These curves only indicate the general convergence behavior through their shape. The general behavior is sufficient for comparison purposes since local fluctuations may be due to inherent properties of one specific mesh or the switching from one convergence mode to the other and thus should not be considered characteristic of the general problem.

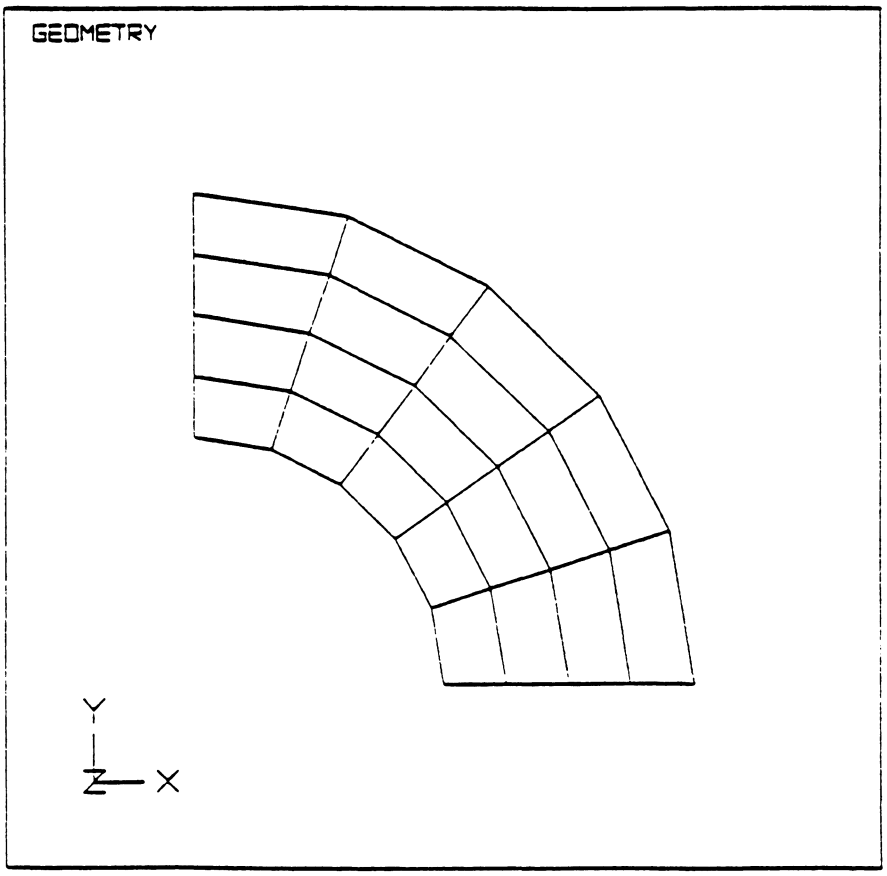

Figure 5-3. Starting Mesh of First Test Case

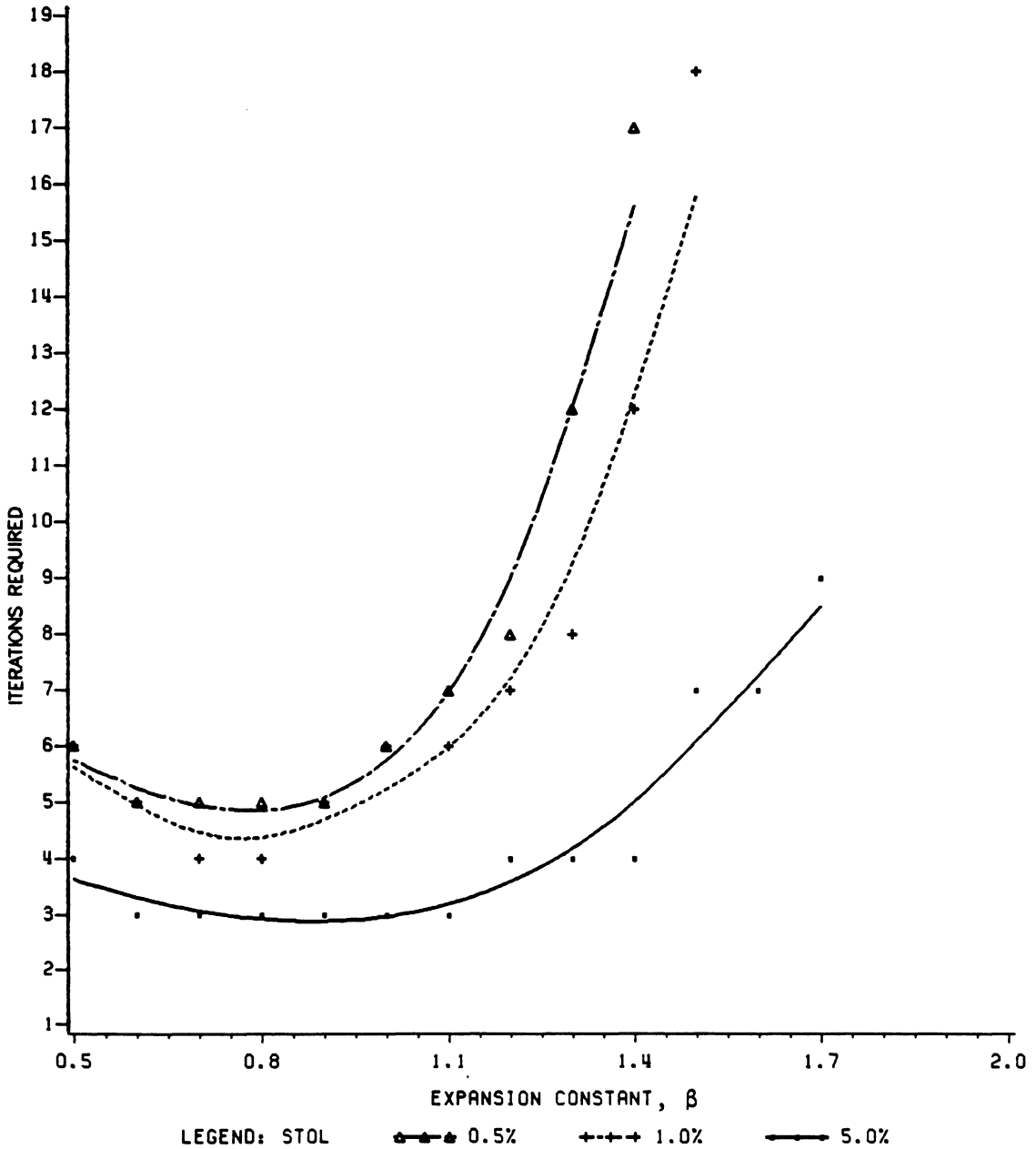

Figure 5-4. Convergence Behavior of First Test Case with SE Criterion

All three curves in Fig. 5-4 exhibit a minimum, as predicted. For STOL values of 0.5% and 1.0%, the curves reach their minima at a β of 0.75 and rise sharply as β increases above 0.8. For STOL of 5.0%, however, the curve is flatter and the minimum is not reached until β reaches 0.85. However, due to the flatness of the curve and the indication of the data points, the range of acceptable β values is between 0.6 and 1.1. Thus, 0.75 can be selected as the optimal β in this test case since the mesh converges fastest for this β, regardless of the STOL used.

One comment should be made on the relative positions of the minima of the three curves. Notice in Fig. 5-4 that the minimum tends to move to lower values of β as the value of STOL decreases, making the convergence criterion stricter. The reason for this phenomenon is that when β increases above a certain value, the convergence becomes oscillatory due to fluctuations of the mesh from iteration to iteration. A stricter convergence criterion allows less fluctuations than a loose criterion; and therefore, the minimum tends to shift towards the monotonic convergence region. Further note that while all three curves terminate due to divergence, the curve for STOL = 0.5% terminates first, followed by those for STOL = 1.0% and 5.0%. This variation in divergence point is also due to the fact that a stricter convergence criterion tolerates less fluctuations in the mesh.

The results of the convergence study using the DSE criterion are plotted in Fig. 5-5, again for STOL of 0.5%, 1.0%, and 5.0%. Similar to the curves of the strain energy method, the curves in Fig. 5-5 also exhibit minima in the vicinity of β = .75. As before, the curve for STOL = 5.0% is flatter and has a wider range of acceptable values of β. The

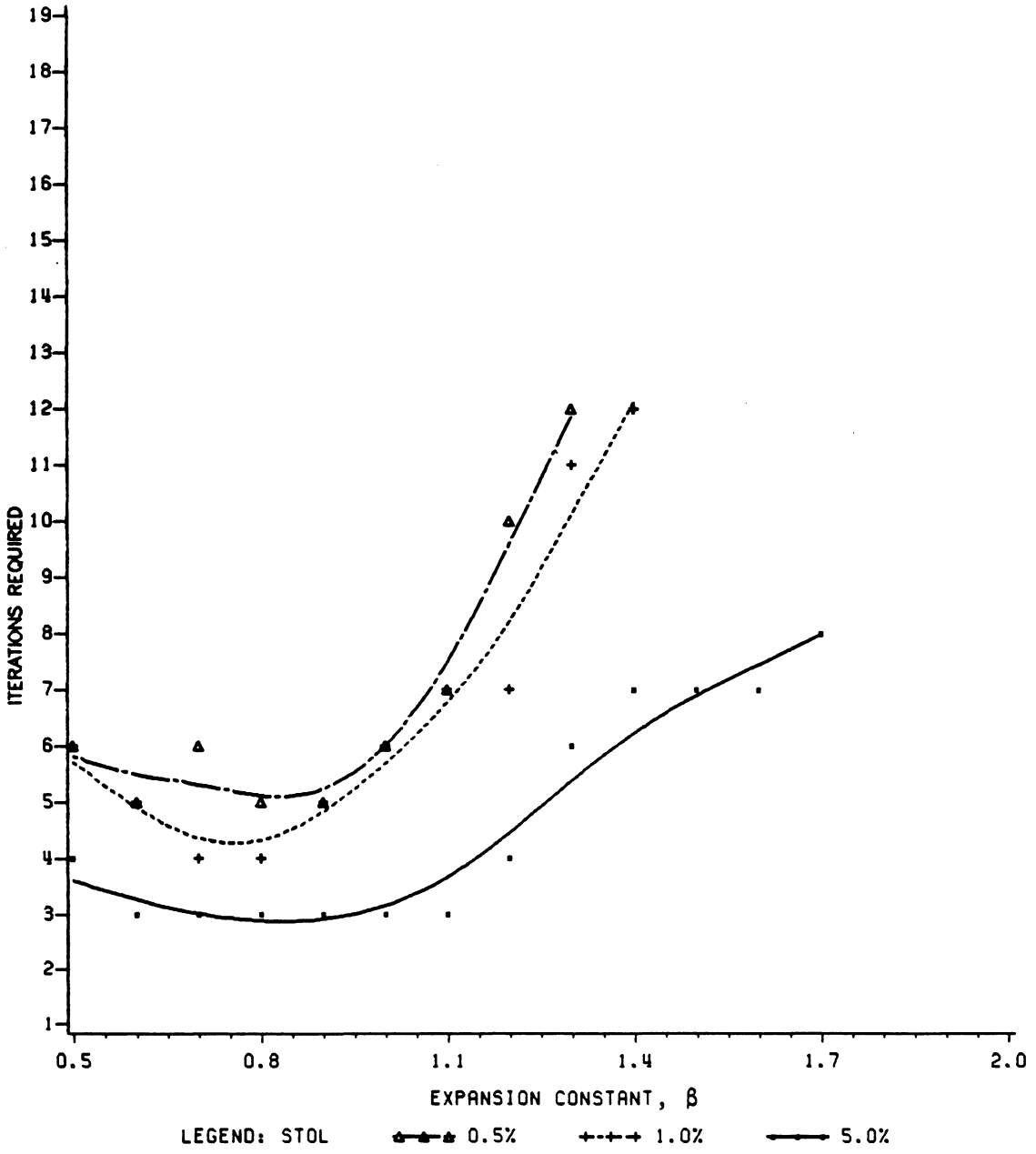

Figure 5-5. Convergence Behavior of First Test Case with DSE Criterion

curves of the two methods are not only similar in shape and divergence points but also in numerical values of the minima, as evident from Figs. 5-4 and 5-5. Therefore, the choice of β for this test case is independent of the method used. The optimal values of β are the same for both methods.

Although the optimal value of β is 0.75 for both methods in this test case, other values of β also yield reasonable convergence rates. In particular, the range of β from 0.5 to 1.0 yields convergence rates not too much slower than the minimum. In this range, the maximum number of iterations required is only 6 for STOL = 0.5% and STOL = 1.0%, and 4 for STOL = 5.0%. Therefore, all values of β in this range can be considered acceptable for both methods.

5.1.2. Second Test Case

Similar to the first test case, only a quarter of the bar needs to be modeled due to symmetry of the problem. Again, a coarse mesh is used to model the upper right corner of the bar, as shown in Fig. 5-6. Only 15 elements are used for this model. Notice that the variation in the element sizes of this starting mesh is fairly large, due to inherent geometrical characteristics of the bar and the method of mesh generation employed. While there is a definite size distribution in this initial mesh, it may not be the same as the optimum mesh which will be reached after the optimization process. Again, the elements are assumed to have the following material properties:

Young's Modulus = 30×10^6 psi (207 GPa)

Poisson's Ratio = 0.3

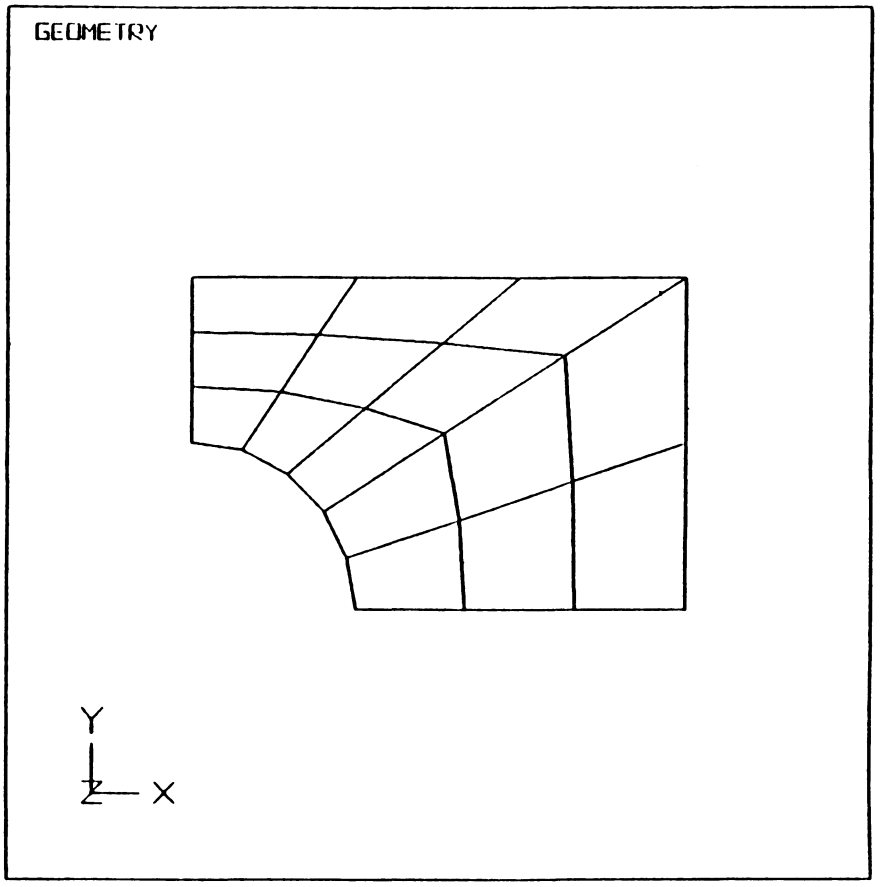

Figure 5-6. Starting Mesh of Second Test Case

Like the first test case, the nodes along the axes of symmetry were confined to sliding along the axes of symmetry in the actual problem. For the expansion problem, the nodes along the horizontal edge of the bar were confined to sliding along the edge only. The loading constraints of the expansion also required the nodes on the vertical edge, being subjected to external loads, to be constrained from all displacements. Furthermore, the three lowest nodes on the arc are fixed to retain the curvature of this critical part of the hole so that the stress flow in this area will not be perturbed.

The results of the convergence study on this test case, using the SE criterion, are plotted in Fig. 5-7 for STOL's of 0.5%, 1.0%, and 5.0%. Again, smooth curves are faired through the data points to indicate the general behavior of the data. The curve for STOL = 0.5% terminates at β = 1.4 due to divergence. However, the curve has leveled out after β reached 1.2. Thus, the minimum of this curve can be considered as occurring at β = 1.2. Similarly, the the minimum of the STOL = 1.0% curve occurs at a β of 1.2, before divergence occurs. The curve for STOL = 5% , however, stays flat at the minimum from β = 0.5 to β = 1.8 and then rises up before stopping at a β of 1.9. Like the first test case, the minimum of this test case also tends to move towards lower values of β as the convergence criterion becomes stricter. Unlike the first test case, however, the optimal β is in the vicinity of 1.2, rather than 0.75.

The results of the convergence study involving the second test case and the DSE criterion are plotted in Fig. 5-8. These results are, again, remarkably similar to those from the SE criterion. The minima of the curves STOL = 0.5% and STOL = 1.0% are identical to those of the SE cri-

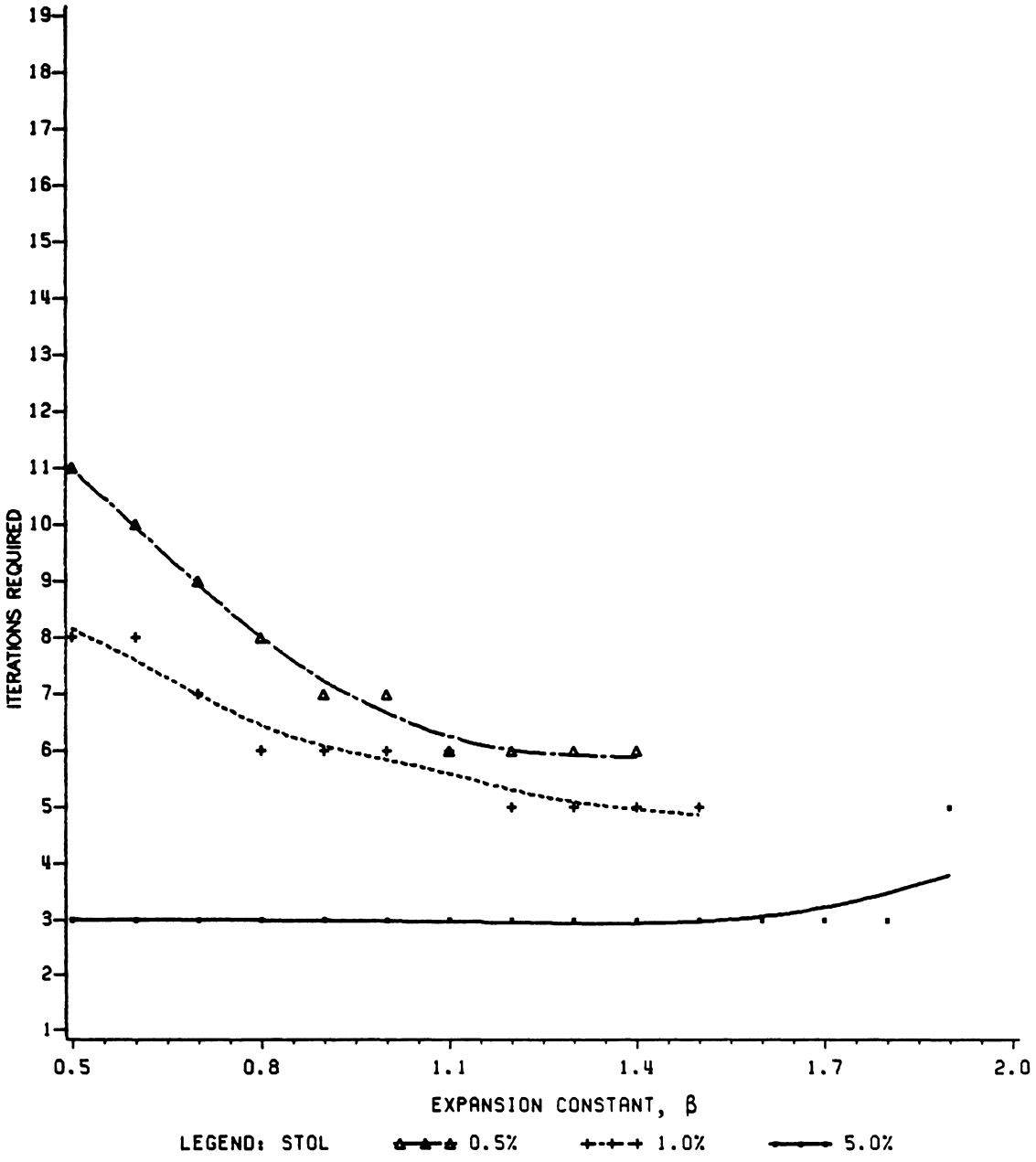

Figure 5-7. Convergence Behavior of Second Test Case with SE Criterion

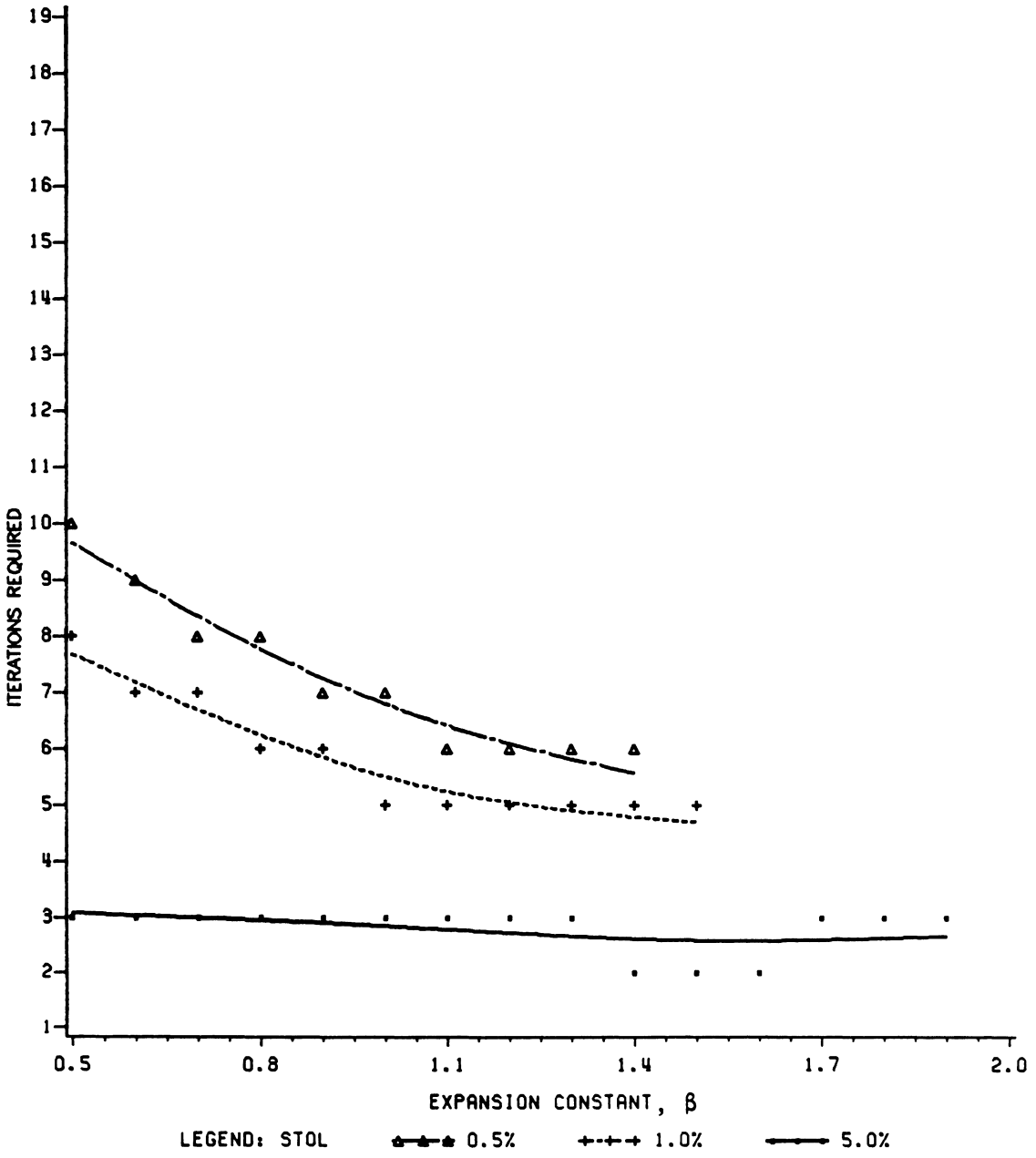

Figure 5-8. Convergence Behavior of Second Test Case with DSE Criterion

terion in both magnitude and location. The minimum of the curve STOL = 5.0% is only slightly different from that of the SE criterion in that it occurs at $\beta = 1.5$ and has a magnitude of 2, rather than 1.4 and 3, respectively. However, this is a very small difference and can be ignored for all practical purposes.

From the results above, it can be observed that the convergence behavior of this test case, like the first test case, is almost identical for both criteria. Again, a common range of β's which yields reasonable convergence rates can be selected for both criteria. For the second test case, this range can be chosen to be from 0.9 to 1.4, for which the maximum number of iterations required is 7 for STOL = 0.5%, 6 for STOL = 1.0%, and 3 for STOL = 5.0%.

Notice that range of acceptable value of β is higher for the second test case which has a stress concentration than for the first test case which has no stress concentrations. This phenomenon can be explained very simply because the elements in the vicinity of the stress concentration need to shrink a greater amount than areas without stress concentration. Even though the normalization of the coefficient of expansion creates a higher compressive strains for these elements they are still not high enough to cause the necessary amount of shrinkage of the elements in each iteration to yield the same convergence rate as that of problems with no stress concentrations. Therefore, β must be increased to boost the compressive strains still higher.

Although the optimal value of β for the second test case is different from that for the first test case, the intersection of the acceptable ranges of the two test cases can be taken to be the acceptable range for

both test case, and by generalization, for most engineering problems. This range of β is from 0.9 to 1.0. In this range, it takes a maximum of 6 iterations for the first test case and a maximum of 7 iterations for the second test case to reach a STOL of 0.5%, for both optimization criteria. While these numbers of iterations may not be the minimum for each test case, they are small enough to be considered practical. The possible increase in number of iterations is however compensated by the assurance of convergence for all problems.

5.2. Evaluation of Results

Now that the convergence behaviors have been studied, it remains to be verified that the optimum meshes generated for each test case using both criteria actually yield more accurate results than the starting meshes. In this section, the results of the optimum meshes of each test case are to be compared against those of the corresponding starting mesh and with the theoretical solutions to see if the optimization process did improve the accuracy of the results. The two criteria are compared against each other in each test case an attempt to decide on the better criterion of the two. For comparison, the same values of β and STOL were used for both test cases and both criteria. A β of 0.9 and a STOL of 0.5% are chosen for the evaluation of results.

5.2.1. First Test Case

The analytical solutions of the vessel with internal pressure can be obtained from classical elastic theories. Figure 5-9 shows the stress components in the wall of the cylinder. σ_l is the longitudinal stress due to the pressure of the ends of the vessel. σ_h and σ_r are the hoop stress and the radial stress, respectively, due to the pressure on the inner surface of the cylindrical wall. Since only a cross section of the wall is modeled, only stresses σ_h and σ_r are involved in this problem. Through analytical methods, Timoshenko [16] found the expression for σ_h and σ_r in terms of the inner and outer radii, the internal pressure, and the radius of interest r:

$$\sigma_h = \frac{Pa^2(b^2 + r^2)}{r^2(b^2 - a^2)} \tag{5.1}$$

$$\sigma_r = \frac{Pa^2(r^2 - b^2)}{r^2(b^2 - a^2)} \tag{5.2}$$

where a is the inner radius,
b is the outer radius,
r is the radius of interest, and
P is the internal pressure.

Substituting numerical values into these equations, the hoop stress and the radial stress as functions of r are shown in Fig. 5-10. The hoop stress is tensile and has a maximum value of 16.67 kpsi (114.9 MPa) at

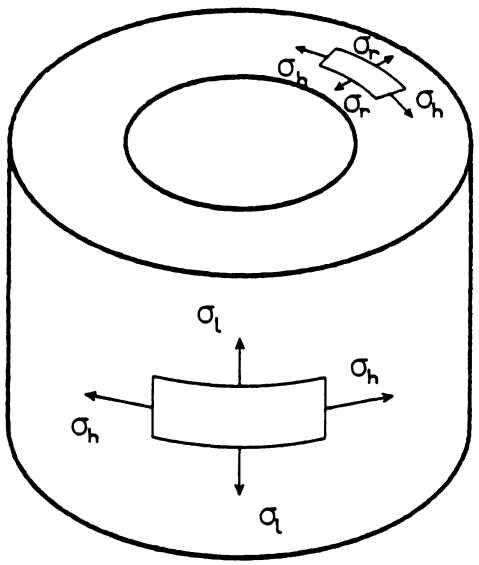

Figure 5-9. Stress Components in a Pressure Vessel Wall

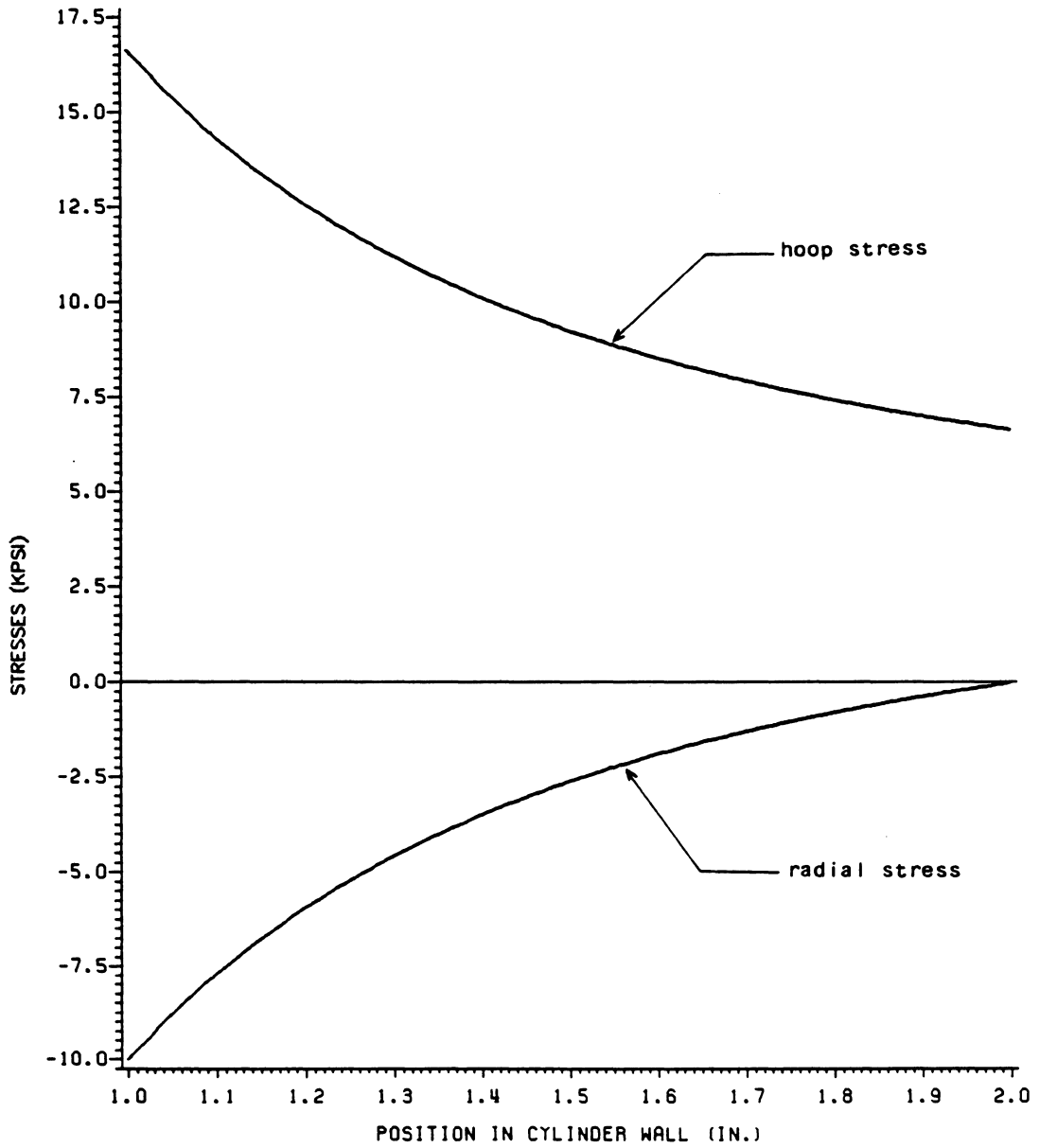

Figure 5-10. Stresses in Vessel Wall due to Internal Pressure

the inner radius and then tapers off to 6.67 kpsi (46.0 MPa) at the outer radius. The radial stress is compressive and has a maximum of -10.0 kpsi (-68.9 MPa) at the inner radius and reduces to zero as r reaches to outer radius. The maximum hoop stress and the maximum radial stress are considered design stresses and will be used as comparison parameters for this test case.

The starting mesh of this test case, shown previously in Fig. 5-3, is shown again here in Fig. 5-11 to refresh the reader. The x stress contour plot for this mesh is shown in Fig. 5-12. The maximum hoop stress is the same as the x stress at the intersection of the vertical axis of symmetry and the inner arc, near contour level G. The maximum compressive x stress located at the intersection of the horizontal axis of symmetry and the inner arc, near contour level A, corresponds to the maximum radial stress in the vessel wall. The contour levels are shown at the upper left corner of the figure. The maximum and minimum levels are only 95% of the actual maximum and minimum stress magnitudes. Thus, the maximum hoop stress is 17.57 kpsi (121.1 MPa). Compared to the theoretical value of 16.67 kpsi (114.9 MPa), the maximum hoop stress calculated from the original mesh has an error of 5.4%. This error is very small considering the non-optimality of the mesh. The maximum radial stress has a magnitude of -6.18 kpsi (-42.6 MPa). Compared to the theoretical value of -10.0 kpsi (-68.9 MPa), the calculated value contains an error of 38.2%!

The SE criterion yields the optimum mesh shown in Fig. 5-13 after 5 iterations. Note that the high stresses, and subsequently high strain energy densities, at the inner radius cause the inner elements to shrink considerably. Moving away from the inner radius, the stresses decrease

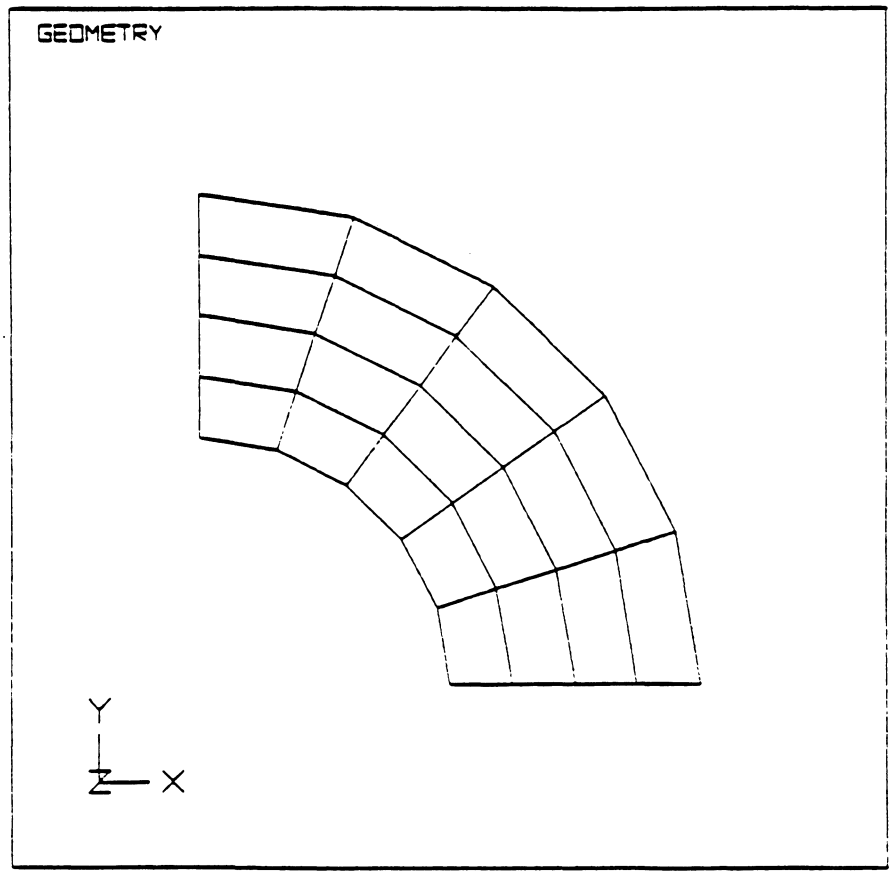

Figure 5-11. Starting Mesh of First Test Case (Repeated)

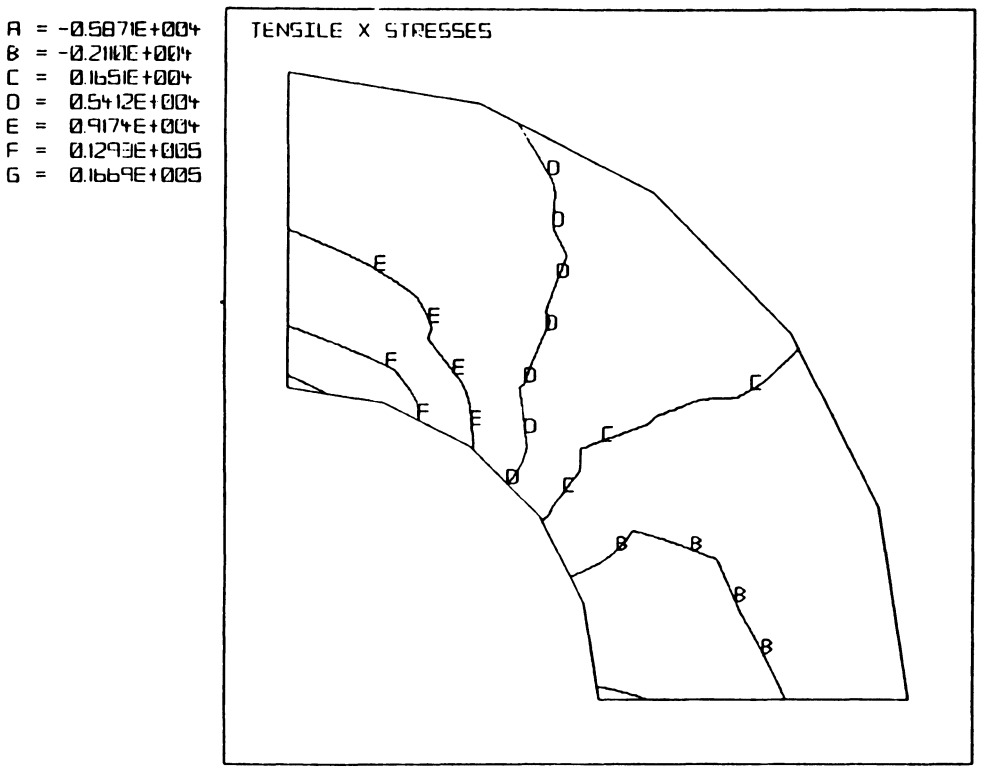

Figure 5-12. X Stress Plot for Starting Mesh of First Test Case

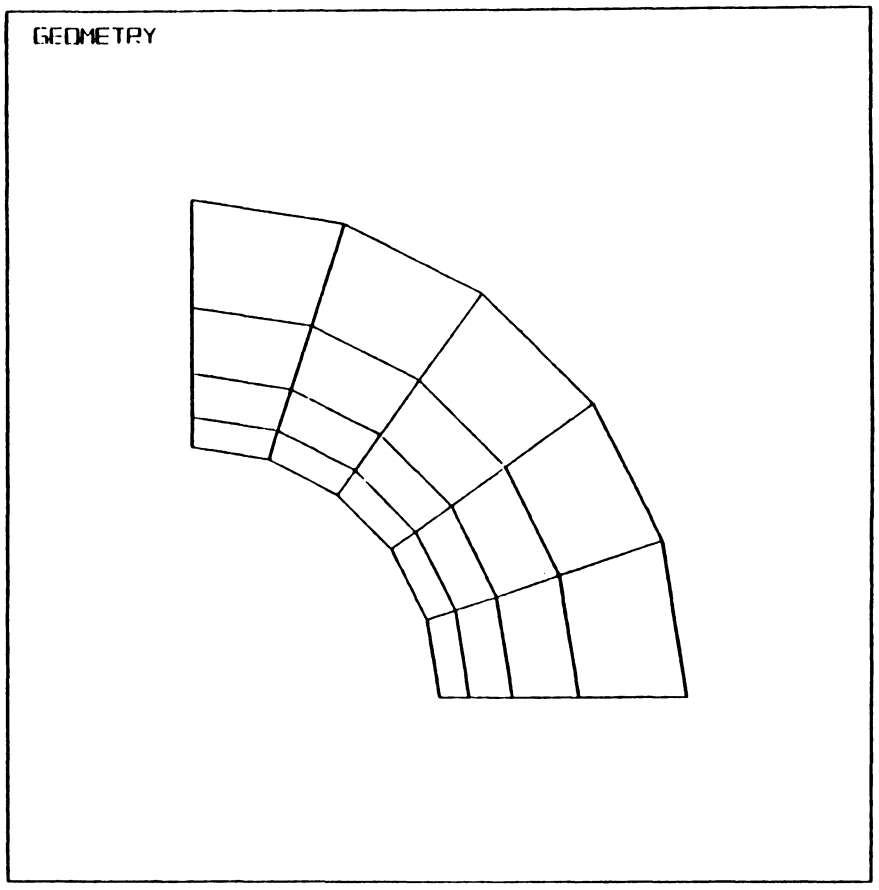

Figure 5-13. Optimum Mesh of First Test Case -- SE Criterion

and the elements increase in size until the outer radius is reached. The x stress contour plot for this optimum mesh is shown in Fig. 5-14. Again, the maximum and minimum contour levels are only 95% of the actual maximum and minimum stresses. The maximum hoop stress is 17.25 kpsi (118.93 MPa), or an error reduction of 35.6% over the starting mesh. Also, the maximum radial stress improves drastically from -6.18 kpsi (-42.6 MPa) in the starting mesh to -7.69 kpsi (-53.0 MPa) in the optimum mesh. This is an error reduction of 39.5%. Note that there is still an error of 3.5% in the maximum hoop stress and -20.4% in the radial stress due to the limited number of elements used.

The DSE criterion yields an optimum mesh also after 5 iterations. This optimum mesh, shown in Fig. 5-15, is nearly identical to the optimum mesh obtained from the SE criterion. In fact, when the meshes are overlain one on top of the other, the innermost elements are identical in size. The sizes of the outer elements differ slightly for the two methods but the differences are barely noticeable. The x stress contour plot for the optimum mesh of the DSE criterion is shown in Fig. 5-16. The maximum hoop stress is 17.24 kpsi (118.86 MPa), which represents an error reduction of 36.6% over the starting mesh. This improvement is slightly better than that of the SE criterion, which is 35.6%. The maximum radial stress is -8.03 kpsi (-55.5 MPa), which is an error reduction of 48.4% over the starting mesh. Again, this improvement is slightly better than that of the strain energy criterion (39.5%).

The comparison of the two criteria can be greatly facilitated by the plot of the maximum stresses in each iteration against the iteration number. Figure 5-17 shows the maximum hoop stress as function of step

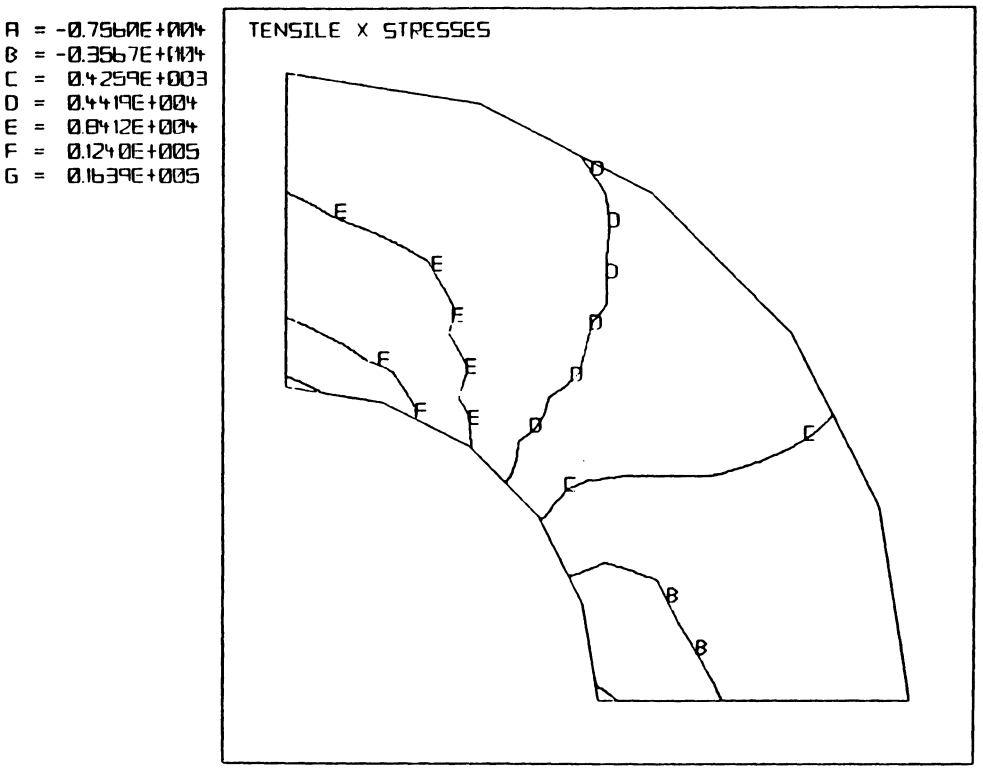

Figure 5-14. X Stress Plot for Optimum Mesh of First Test Case -- SE Criterion

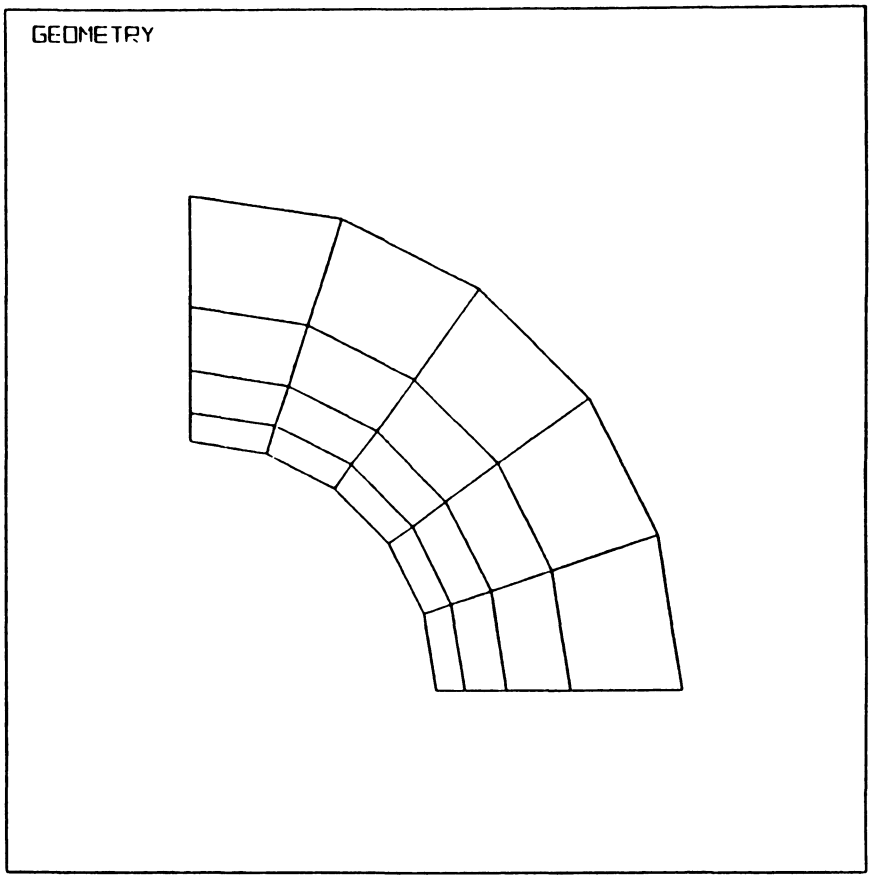

Figure 5-15. Optimum Mesh of First Test Case -- DSE Criterion

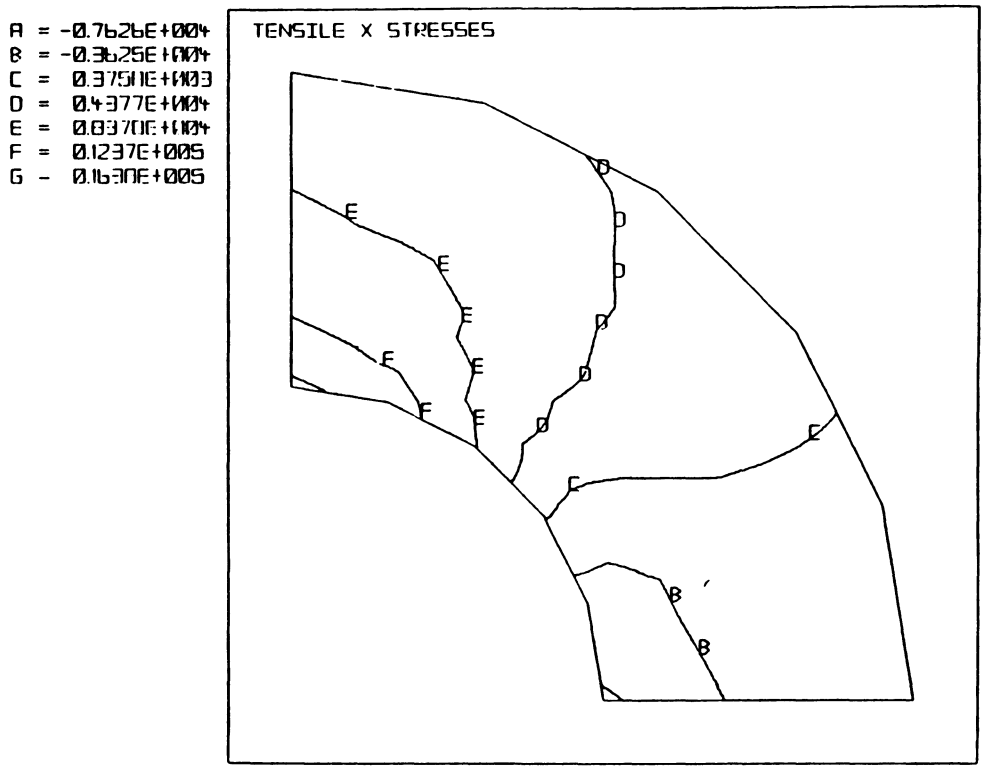

Figure 5-16. X Stress Plot for Optimum Mesh of First Test Case -- DSE Criterion

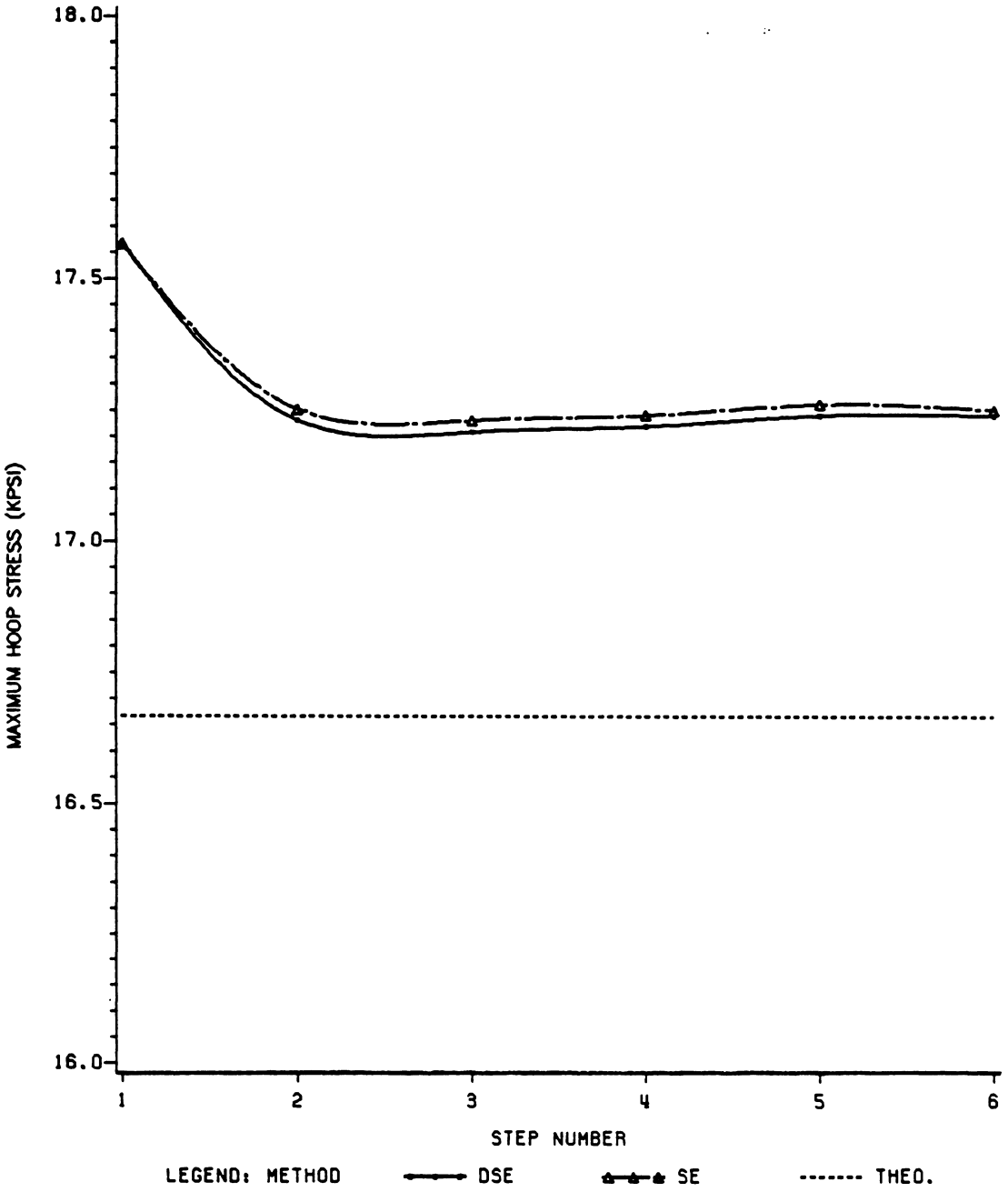

Figure 5-17. Improvement in Maximum Hoop Stress

number for both criteria. The starting mesh is step 1 and the optimum mesh, after 5 iterations is step 6. Similarly, Fig. 5-18 shows the curves of maximum (compressive) radial stresses. It is evident from these figures that the deviatoric strain energy yields slightly but consistently lower tensile stresses and higher compressive stresses. In other words, the curves using deviatoric strain energy method always lie below those using strain energy, and thus closer to the theoretical values for this test case. Also note that most of the improvements in the maximum stresses occurs after only 1 iteration. The other iterations are needed to improve the stress distribution throughout the wall. Therefore, if only the maximum stresses are of interest, it is not necessary to make STOL too small. For this test case, or other problems with no stress concentrations, a STOL as large as 5.0% may be sufficient to produce accurate maximum stresses.

A remark should be made regarding the magnitude of error in the computed maximum stresses. Recall that the nodal stresses are calculated from the Gauss point stresses by passing a smoothing surface through the latter values. As a result, the nodal stresses contain two sources of error: discretization error and interpolation error. Since the actual stress field may be totally different from the assumed shape of the smoothing surface, the interpolation error can be quite significant when only a few large elements are used as in this case. Consequently, perhaps the centroidal stresses of the innermost element may be better comparison parameters since they are more accurately calculated than the nodal stresses. This comparison is discussed in the following paragraphs.

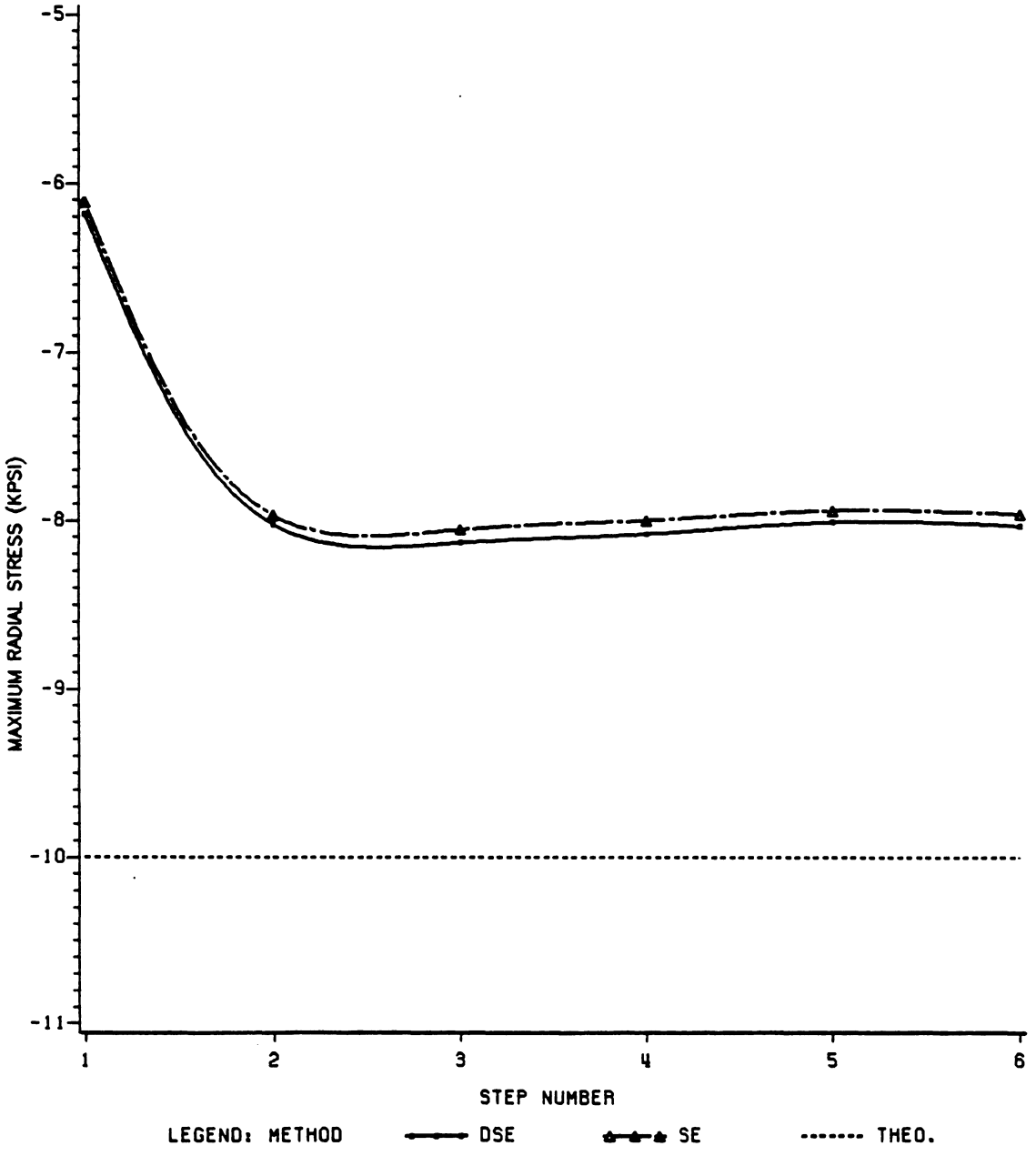

Figure 5-18. Improvement in Maximum Radial Stress

While using the centroidal stresses as a basis for comparison reduces the interpolation error, it presents a new problem. Since the optimization procedure changes the element sizes and shapes from iteration to iteration, the coordinates of the element centroids also change. This phenomenon is illustrated in Figs. 5-19 and 5-20, which show the starting mesh and the optimum mesh obtained using the SE criterion, respectively. The centroids of the elements in one radial row of the starting mesh are labeled as points A, B, C, and D in Fig. 5-19. In the optimum mesh, these centroids have moved to new locations marked by points A', B', C', and D' in Fig. 5-20, respectively. The centroids of the starting mesh are also overlain in Fig. 5-20 to emphasize the motions of the centroids. To make a meaningful comparison the stresses at a chosen point in the starting mesh have to be compared to the stresses at the same point in the optimum mesh, as in the previous comparison of maximum nodal stresses. Since the element centroids in the starting mesh and the optimum mesh do not coincide, the stresses at these points cannot serve directly as comparison parameters. However, the errors in centroidal stresses can be used to deduce any improvement in the optimum mesh in an indirect manner: since point A lies between points A' and B', with the assumption that the error field is uniform, the errors at points A' and B' in the optimum mesh can serve as bounds for the error at A in the same mesh. By comparing these error bounds at point A in the optimum mesh and the error at the same point in the starting mesh, it can be decided whether an improvement was made.

The comparison requires that the x tensile stress, y tensile stress, and xy shear stress at point A in the starting mesh and at points A' and

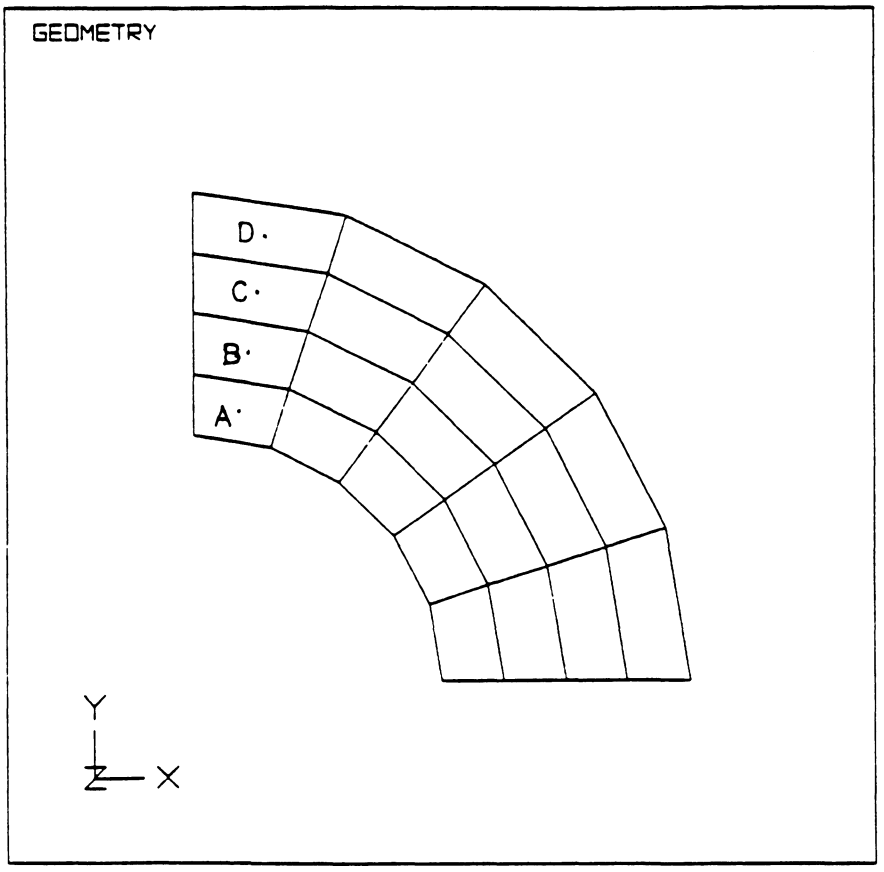

Figure 5-19. Locations of Element Centroids in Starting Mesh

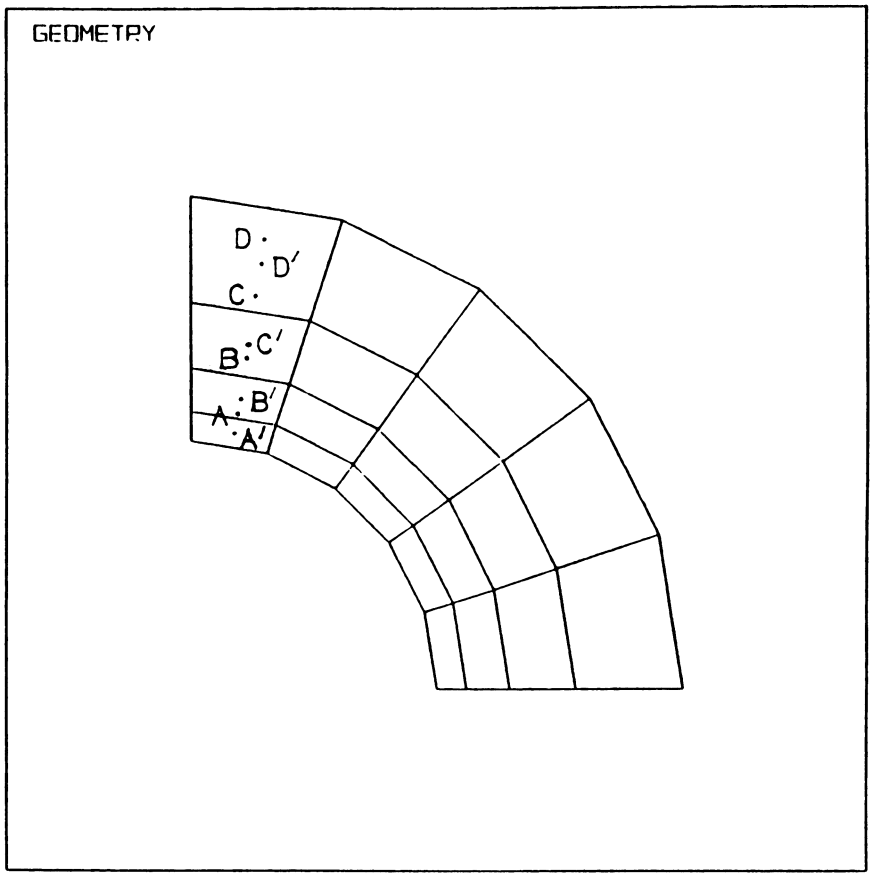

Figure 5-20. Locations of Element Centroids in Optimum Mesh of SE Criterion

B' in the optimum mesh be converted to the hoop and radial stresses. Knowing that the hoop and radial stresses in this case are the principal stresses, they can be calculated according to the following equations taken from Shigley [17]:

$$\sigma_h = \frac{\sigma_x + \sigma_y}{2} + \sqrt{\left(\frac{\sigma_x - \sigma_y}{2}\right)^2 + \tau_{xy}^2} \tag{5.3}$$

$$\sigma_r = \frac{\sigma_x + \sigma_y}{2} - \sqrt{\left(\frac{\sigma_x - \sigma_y}{2}\right)^2 + \tau_{xy}^2} \tag{5.4}$$

where σ_x is the x tensile stress,

σ_y is the y tensile stress,

τ_{xy} is the xy shear stress,

σ_h is the hoop stress, and

σ_r is the radial stress.

The theoretical hoop stress and radial stress at the points can be computed from equations 5.1 and 5.2 with the proper value of r. Then, the errors at point A in the starting mesh and at A' and B' in the optimum mesh can be calculated. The results of these calculations are tabulated in Table 5-1 and Table 5-2 for the SE criterion and the DSE criterion, respectively.

Table 5-1 shows a clear improvement in the stresses at point A. The error in hoop stress has been reduced from 1.93% in the starting mesh to smaller than 1.08% in the SE optimum mesh. Similarly, the error in radial stress decreases from -2.52% to less than -0.41%. Table 5-2 shows similar

Table 5-1. Comparison of Centroidal Stresses Between Optimized Mesh Using SE Criterion and Analytical Method

	INITIAL MESH	SE OPTIMUM MESH	
Location	A	A'	B'
σ_x (psi)	13661	14720	12140
σ_y (psi)	-6674	-7963	-5347
τ_{xy} (psi)	-3304	-3685	-2841
σ_h (psi)	14136	15304	12590
σ_r (psi)	-7199	-8547	-5797
r (in.)	1.1250	1.0609	1.2091
Theo. σ_h (psi)	13868	15179	12453
Theo. σ_r (psi)	-7022	-8512	-5787
Error in σ_h	1.93%	0.82%	1.08%
Error in σ_r	-2.52%	-0.41%	-0.18%

Table 5-2. Comparison of Centroidal Stresses Between Optimized Mesh Using DSE Criterion and Analytical Method

	INITIAL MESH	DSE OPTIMUM MESH	
Location	A	A'	B'
σ_x (psi)	13661	14758	12243
σ_y (psi)	-6674	-8012	-5462
τ_{xy} (psi)	-3304	-3700	-2876
σ_h (psi)	14136	15344	12698
σ_r (psi)	-7199	-8598	-5918
r (in.)	1.1250	1.0586	1.2012
Theo. σ_h (psi)	13868	15230	12574
Theo. σ_r (psi)	-7022	-8564	-5908
Error in σ_h	1.93%	0.74%	0.99%
Error in σ_r	-2.52%	-0.40%	-0.16%

improvements in the DSE optimum mesh: the hoop stress error decreases from 1.93% to less than 0.99% and the radial stress error decreases from -2.52% to -0.40%. The results confirm the improvements seen in the comparison of nodal stresses previously.

The relative effectiveness of the two criteria can also be deduced from a comparison of the stresses at points A' and B' in the two optimum meshes. Notice in Tables 5-1 and 5-2 that while points A' and B' are not at exactly the same locations in the two optimum meshes, the differences in location are so small that the points can be considered to be at the same locations in both meshes for comparison purpose. A comparison of the two tables shows that the DSE criterion yields slightly better results than does the SE criterion, as evident in the smaller errors in both stresses at both locations in the DSE mesh. This observation confirms the slight superiority of the DSE criterion over the SE criterion in this test case, as concluded in the comparison of nodal stresses. Thus, while nodal stresses may contain large interpolation errors, they can be used sufficiently as comparison parameters to test the validity of the method and the relative effectiveness of the two criteria.

5.2.2. Second Test Case

As stated previously, the second test case was chosen for its high stress concentrations at the top and bottom of the center hole. Peterson [18] presents stress concentration factors for the finite width bar of infinite length with a center hole under tensile loads. Although this case has finite length, the stress concentrations are fairly localized

around the top and bottom of the hole and thus the length of the bar does not affect the results significantly. The stress concentration factor K_t is defined by Peterson as:

$$K_t = \frac{\sigma_{max}}{\sigma_o} \tag{5.5}$$

where σ_{max} is the maximum stress at the top and the bottom of the hole and σ_o is the average stress in the web section. Peterson plotted the stress concentration factor as a function of the ratio of the hole diameter a to the bar width w. For this test case, the ratio a/w is 0.5 and the corresponding stress concentration factor is 2.16. This stress concentration factor is the same for the top and the bottom of the hole due to symmetry of the problem.

The starting mesh of this test case was shown in Fig. 5-6 and repeated here in Fig. 5-21. Since the stress concentration factor involves primarily the stresses in the x direction, only the contour plot of this stress component is of interest. The x stress contour plot for the starting mesh is shown in Fig. 5-22. The maximum stress occurs near contour level G, which is located at the intersection of the vertical line of symmetry and the arc. This stress is calculated to be 38.9 kpsi (268 MPa), yielding a stress concentration factor of 1.94. This value is significantly lower than the theoretical value of 2.16, and in error by -10.0%. Furthermore, the minimum x stress is incorrectly calculated to be a negative value in Fig. 5-22 when the whole bar is supposed to be in tension in the x direction.

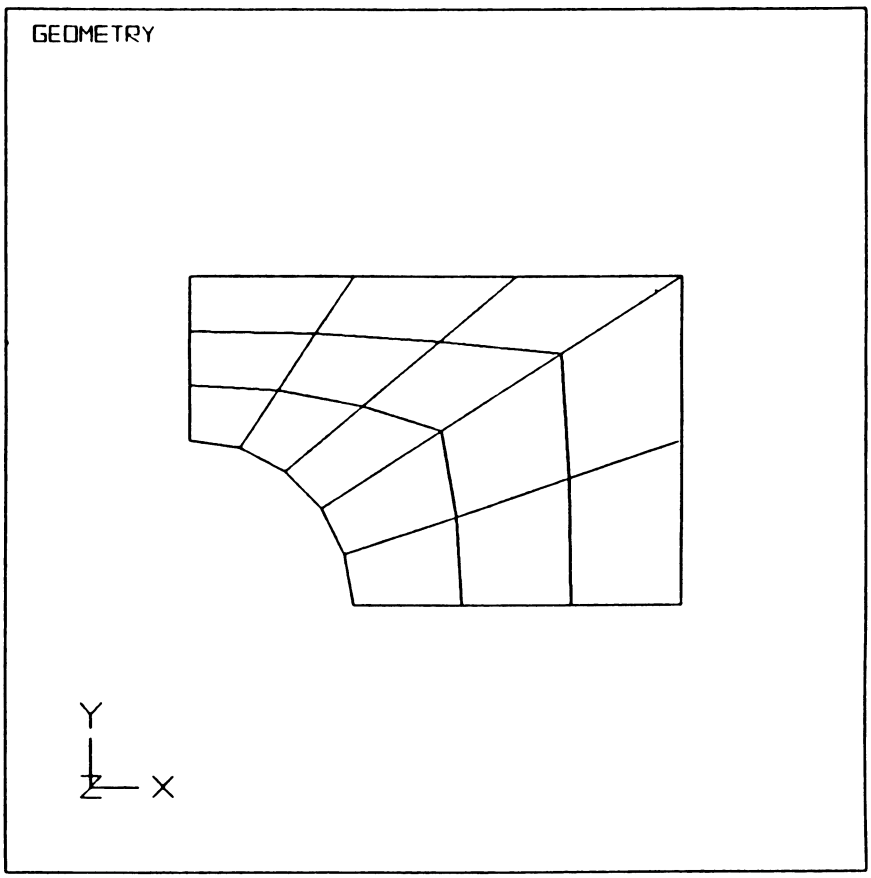

Figure 5-21. Starting Mesh of Second Test Case (Repeated)

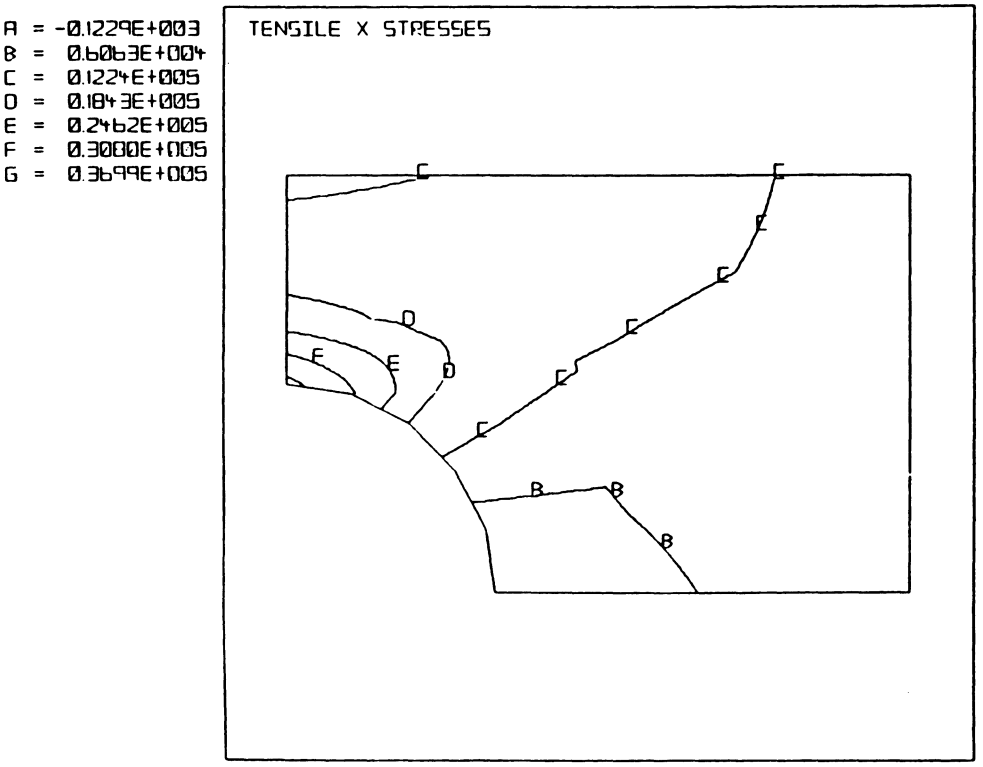

Figure 5-22. X Stress Plot for Starting Mesh of Second Test Case

The optimum obtained by the SE criterion after 7 iterations is shown in Fig. 5-23. The elements near the stress concentration underwent considerable shrinkage while those farther away expanded. Also notice how the curvature of the hole is preserved by fixing the three lowest nodes on the arc. The stress contour plot of this optimum mesh is shown in Fig. 5-24. The maximum stress now becomes 42.5 kpsi (293 MPa), yielding a stress concentration factor of 2.12. This result is very close to the theoretical value of 2.16, with an error of only -1.6%, as compared to -10.0% in the starting mesh. Thus, a gain of 8.4% has been achieved through the optimization process. Also notice that the minimum contour level has now become a positive value, which is more probable than the negative value of the starting mesh.

The DSE criterion yields the optimum mesh shown in Fig. 5-25 after 7 iterations. This optimum mesh is very similar to that of the SE criterion. The elements in the vicinity of the stress concentration have identical sizes and shapes for both criteria. The elements farther away are only slightly different for the two criteria. The x stress contour plot using the optimum mesh of Fig. 5-25 is shown in Fig. 5-26. The maximum stress obtained from this method is 42.2 kpsi (291 MPa), yielding a stress concentration factor of 2.11, which represents a deviation of -2.3% from the theoretical value. Thus, a gain of 7.7% was made using the DSE criterion, slightly less than the SE criterion.

Like the first test case, the difference in the results of the two criteria are more easily seen in the plot of the maximum stress versus step number for both criteria in Fig. 5-27. As can be seen in the figure, the curve using SE always lies above the curve using DSE and thus, for

Figure 5-23. Optimum Mesh of Second Test Case -- SE Criterion

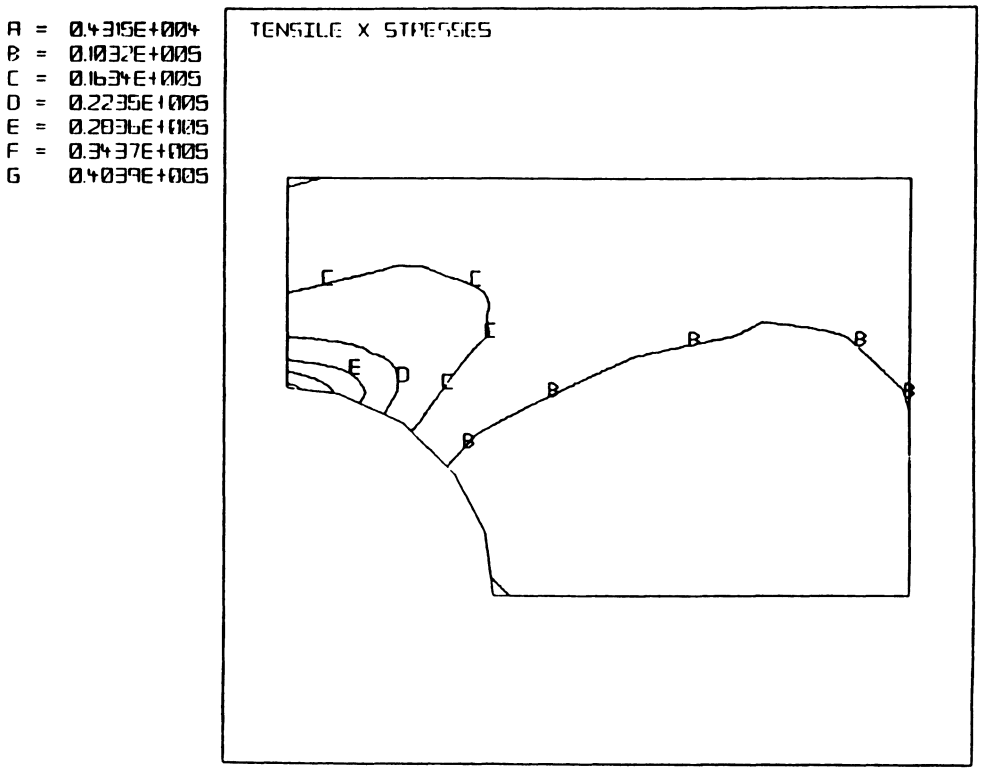

Figure 5-24. X Stress Plot for Optimum Mesh of Second Test Case -- SE Criterion

Figure 5-25. Optimum Mesh of Second Test Case -- DSE Criterion

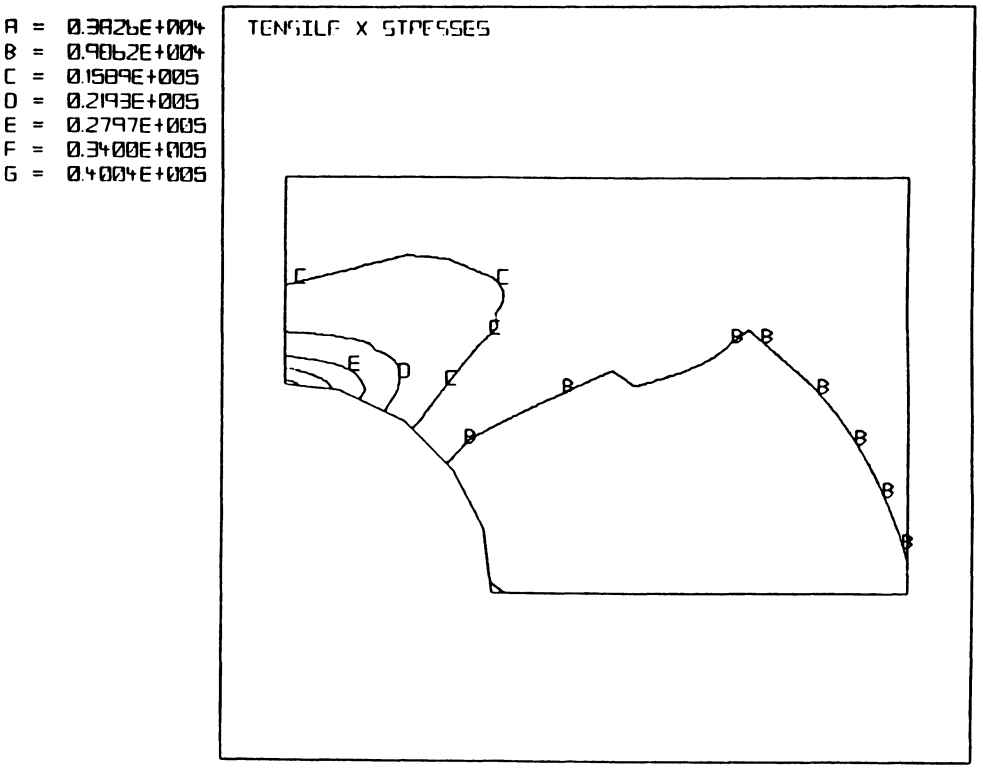

Figure 5-26. X Stress Plot for Optimum Mesh of Second Test Case -- DSE Criterion

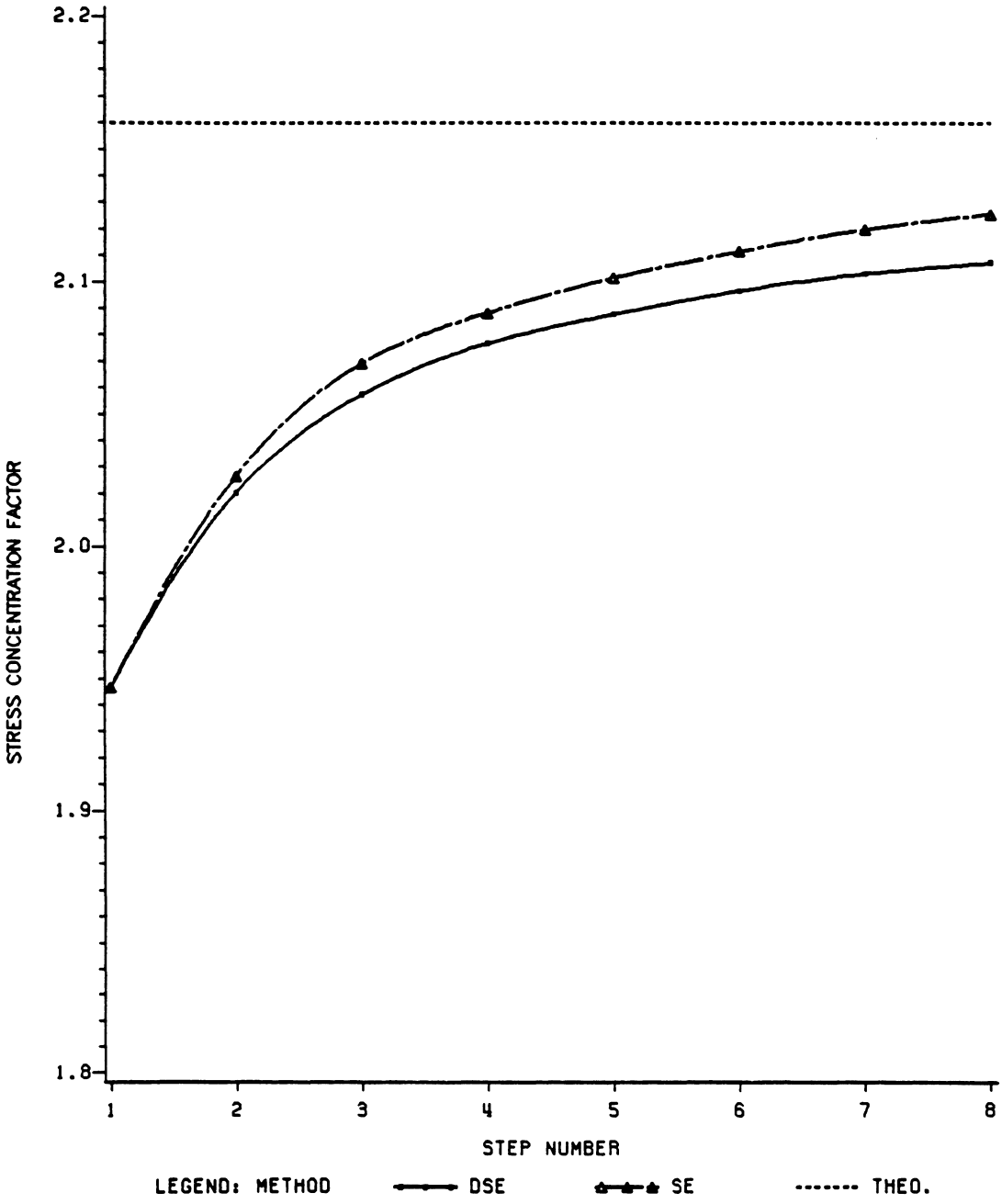

Figure 5-27. Improvement in Stress Concentration Factor

this test case, closer to the theoretical result. In fact, the gap between the curves actually increases with each iteration, signifying that the result using DSE can never catch up with that using the SE criterion.

Also note that the curves start out fairly steep and then level off at the end, implying that most of the improvement was made in the first few iterations. As a matter of fact, in step 4, which corresponds to a STOL of 5.0%, the error in the stress concentration factor is only 3.3% for the SE criterion and 3.8% for the DSE criterion, representing gains of more than 7%, in contrast to an additional gain of only about 2% in the next four iterations! Therefore, as in the first test case, a STOL of 5% is quite adequate.

5.3. Modeling of Problems with Concentrated Loads

Concentrated loads present special problems for the optimization method. Since a concentrated load results in infinite stresses at the point of application, the element or elements containing the point of load application on a node will try to shrink to zero size. This problem calls for special additional boundary conditions in the expansion problem.

Consider a plate with four in plane corner loads as shown in Fig. 5-28. The upper right quarter of the plate is modeled as shown in Fig. 5-29. The use of a small element in the corner of the load will be explained in a later part of this section. Again, appropriate boundary conditions and geometrical constraints are applied to the problem to preserve symmetry and overall problem geometry.

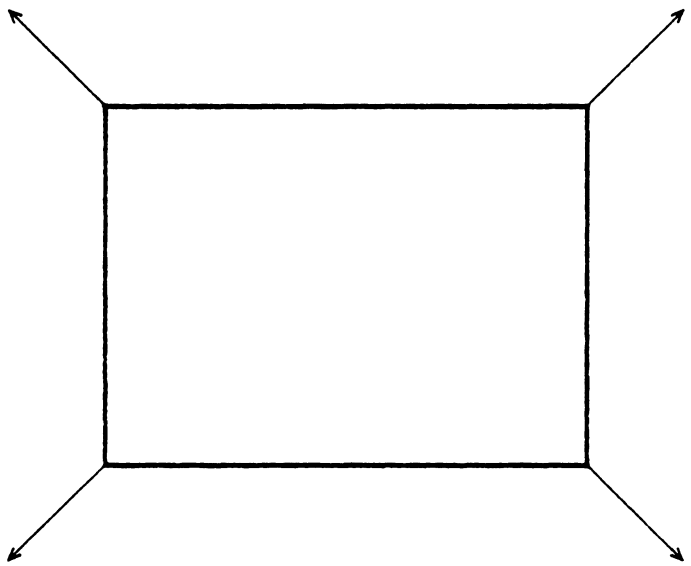

Figure 5-28. Plate with Concentrated Corner Loads

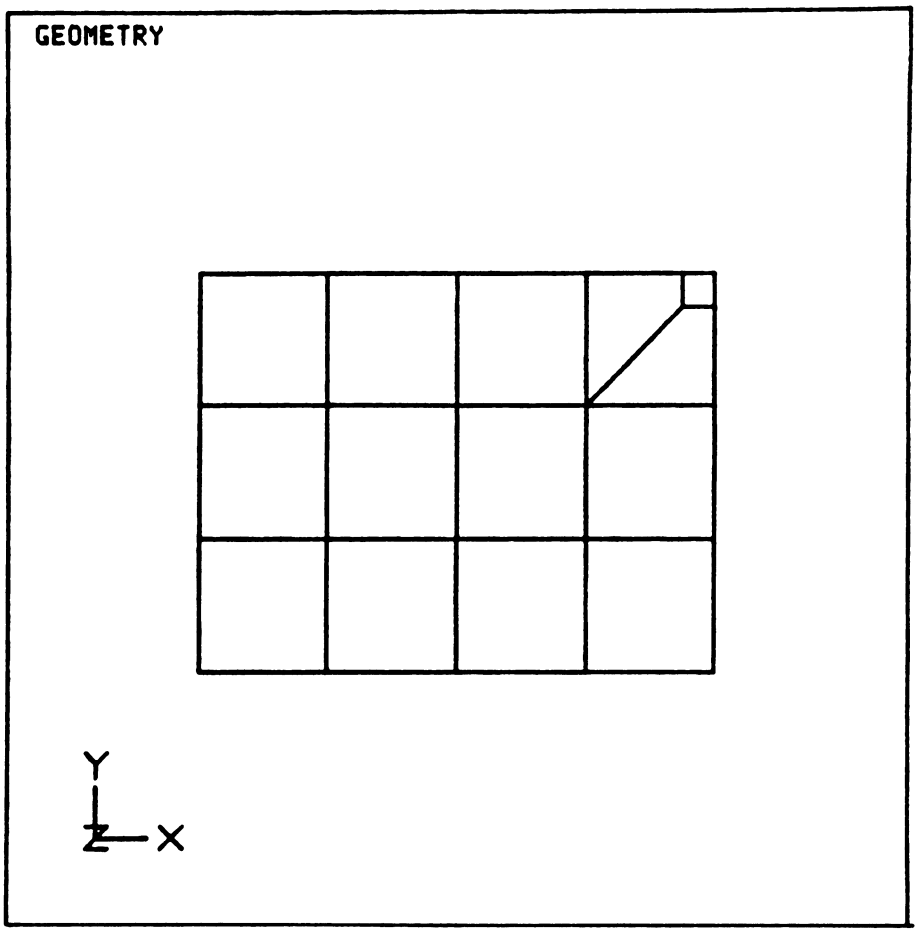

Figure 5-29. Starting Mesh of a Plate with Concentrated Corner Loads

If the two boundary nodes adjacent to the load are free to slide along their boundaries, the corner element will collapse to zero size. The only way to prevent this collapse is to fix these two nodes. However, these restrictions are still insufficient to eliminate the problem caused by the concentrated load. This will be shown in the following discussion.

The mesh, with the two boundary nodes adjacent to the load fixed, is run through the SE optimization method. After 2 iterations, the corner element acquires an inverted angle, i.e., an internal angle greater than 180°. This phenomenon is illustrated in Fig. 5-30. The corner element now becomes a 'bad' element, resulting in an invalid formulation of the stiffness matrix. In order to prevent this problem, it is necessary to fix the remaining node of the corner element as well as the other nodes. As a result, the size and shape of the corner element is not allowed to change at all. This requires the user to select the corner element size which limits the stress level to a practical value so that other elements are not adversely affected. Also, since the corner element does not change in size from iteration to iteration, its energy content must be excluded from the calculations of $GECI_{max}$ and $GECI_{ave}$ so that the initial strains of other elements and the numerical value of the expansion coefficient will not be adversely affected.

When the fourth node of the element is constrained, the mesh converges in 7 iterations for STOL = 1.0% and 9 iterations for STOL = 0.5%, both for a β of 0.9. Notice that strict convergence criterion must be used for this type of problem since the biggest variation in the convergence criterion has been eliminated in fixing the corner element, thus leaving the other variations dwarfed by the high centroidal GEDIs in the vicinity

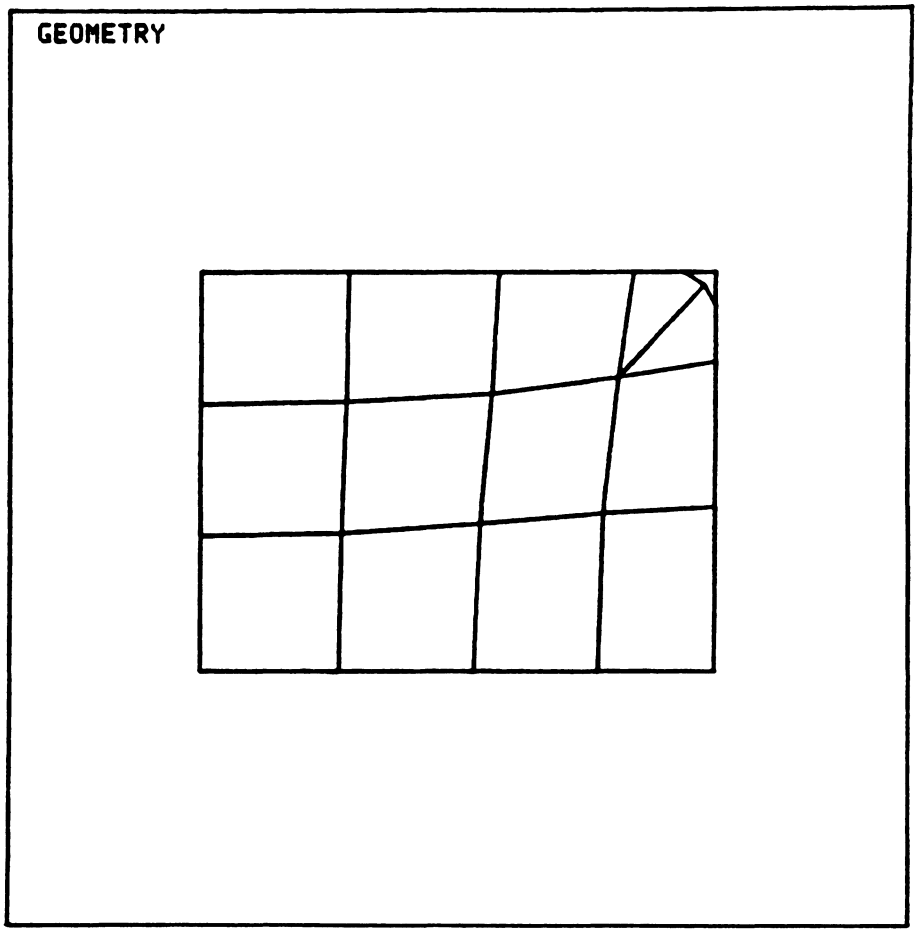

Figure 5-30. Effect of Concentrated Load on Corner Element

of the concentrated load. The optimum mesh for STOL = 0.5% is shown in Fig. 5-31.

In conclusion, to model a problem with concentrated loads, one needs to follow these steps:

1. Select a sufficiently large size for all elements which have a concentrated load.

2. Then, in the expansion problem, fix all nodes of these elements, in addition to the normal geometrical constraints.

Figure 5-31. Optimum Mesh of a Plate with Concentrated Corner Loads

6. CONCLUSIONS

The following conclusions can be drawn from the results of the case studies:

1. The optimization procedure improves the results of the two test cases in only a few iterations. The errors in the maximum stresses in the first test case are reduced by more than 1/3 after only 1 iteration. The error in the stress concentration factor in the second test case is reduced by more than 3/4 after 7 iterations.

2. Both the SE criterion and the DSE criterion yield better results than the unoptimized mesh. The DSE method yields better results than does the SE criterion in the first test case while the reverse is true for the second test case. Therefore, it is difficult to say that one criterion is superior to the other for the general case.

3. The range of β from 0.9 to 1.0 yields reasonable convergence rates for both test cases, and seems to be acceptable for most problems. In problems with stress concentrations, a higher β yields faster convergence rates. In problems with no stress concentrations, a lower β should be used for fastest convergence.

4. A convergence tolerance of 5.0% is adequate for these problems, with or without stress concentrations. However, for problems with con-

centrated loads, a stricter convergence criterion should be used to ensure improvement in accuracy away from the concentrated loads.

5. Since the elements are free to change in size and shape, it is conceivable that some structures may have a highly irregular stress field that can cause excessive distortion of the elements when optimized, thus worsening the accuracy of the results. These problems cannot be optimized by the method unless the element distortions can be regulated. One possible method of regulating element distortions is to increase the Young's modulus and the Poisson's ratio of distorted elements in the expansion problem to make these elements a lot stiffer than other elements in the mesh and therefore preventing distorted elements from getting further distorted.

7. RECOMMENDATIONS FOR FURTHER STUDIES

This paper presented only the principles of the optimization method and application to the linear 2-D isoparametric plane stress element. To make the method applicable to most engineering problems, future studies of the method should aim at the following:

1. Testing the validity of the method for other 1-D and 2-D elements such as axisymmetric element, constant strain triangular element, plate element, shell element, and so on. Also, the range of acceptable β should be expanded to these elements.

2. Establishing a systematic way to fix certain nodes on arcs and other curved boundaries to preserve curvature.

3. Finding a way to monitor, regulate, and reduce the distortion of elements to prevent excessive distortions.

4. Investigating the possibility of modifying the method for the optimization of design shapes such as interior holes and boundary curvatures by freeing or imposing design restrictions on the nodes on the arcs and let these nodes move until an optimal shape is reached.

LIST OF REFERENCES

1. Shephard, M. S., "Finite Element Grid Optimization - A Review," Finite Element Grid Optimization, ASME Special Publication PVP-38, 1979.

2. McNeice, G. M. and Marcal, P. V., "Optimization of Finite Element Grids Based on Minimum Potential Energy," Journal of Engineering for Industry, Transactions of ASME, Vol. 95, No. 1, pp. 186-190, 1973.

3. Carroll, W. E. and Barker, R. M., "A Theorem for Optimum Finite Element Idealizations," International Journal of Solids and Structures, Vol. 9, pp. 883-895, 1973.

4. Turcke, D. J. and Mcneice, G. M., "A Variational Approach to Grid Optimization in the Finite Element Method," Proceedings of the Conference on Variational Methods in Engineering, Southhampton University, England, 1972.

5. Babuska, I. and Rheinboldt, W. C., "A-Posteriori Error Estimates for the Finite Element Method," International Journal for Numerical Methods in Engineering, Vol. 12, pp. 1597-1615, 1978.

6. Babuska, I., "The Self-Adaptive Approach in the Finite Element Method," The Mathemetics of Finite Element and Application II, MAFELAP, Academic Press, 1975.

7. Carey, G. F. and Humphrey, D. L.,"Residuals, Adaptive Refinements and Nonlinear Iterations for Finite Element Computations," Finite Element Grid Optimization, ASME Special Publication PVP-38, 1979.

8. Turcke, D. J. and McNeice, G. M., "Guidelines for Selecting Finite Element Grids Based on an Optimization Study," Computer and Structures, Vol. 4, pp. 499-519, 1974.

9. Shephard, M. S., Gallagher, R. H., and Abel, J. F., "Experiences with Interactive Computer Graphics for the Synthesis of Optimal Finite Element Meshes," Finite Element Grid Optimization, ASME Special Publication PVP-38, 1979.

10. Jara-Almonte, J., "Synthesis of a Near-Optimum Finite Element Mesh," Master of Science Thesis, Department of Mechanical Engineering, Virginia Polytechnic Institute and State University, 1983.

11. Cook, R. D., Concepts and Applications of Finite Element Analysis, John Wiley and Sons, New York, 1974.

12. Zienkiewicz, O. C., The Finite Element Method, McGraw-Hill, England, 1977.

13. Hinton, E. and Campbell, J. S., "Local and Global Smoothing of Discontinuous Finite Element Functions Using a Least Square Method," International Journal for Numerical Methods in Engineering, Vol. 8, pp. 461-480, 1973.

14. Bathe, K. J. and Wilson, E. L., Numerical Methods in Finite Element Analysis, Prentice-Hall, New Jersey, 1976.

15. Brigham Young University, MOVIE.BYU -- A General Purpose Computer Graphics System, Brigham Young University Computer Science Department, Provo Utah, 1981.

16. Timoshenko, S. , Theory of Elasticity, McGraw-Hill, New York, 1934.

17. Shigley, J. E., Mechanical Engineering Design, Third Edition, McGraw-Hill, 1977.

18. Peterson, R. E., Stress Concentration Factors, John Wiley and Sons, New York, 1974.

The vita has been removed from the scanned document